

Quantitative analysis of the joint variability of rock texture and composition in thin section: The Generalized Griffiths Descriptor and its application to sediment generation from granitoids



Bram Paredis^{a,*}, Gert Jan Weltje^a, William A. Heins^b

^a KU Leuven, Department of Earth and Environmental Sciences, Celestijnenlaan 200E, B-3001 Leuven, Belgium

^b Getech, 3000 Wilcrest Drive, Suite 155, Houston, TX 77042, USA

ARTICLE INFO

Keywords:

Fundamental rock properties
Sediment generation
Quantitative petrography
Compositional data analysis

ABSTRACT

The general protocol for quantitative petrographic description of clastic sediments envisioned by J.C. Griffiths approximately 60 years ago is built on specification of the following five statistically independent fundamental properties of aggregates: modal composition, spatial arrangement, size distributions, shape distributions, and orientation distributions of the elements. Each element is represented by a grain falling into one of an exhaustive set of petrographic classes. We introduce the so-called Generalized Griffiths Descriptor (GGD) which extends this protocol to igneous and metamorphic rocks. Statistical independence of the fundamental properties permits rigorous testing of petrogenetic hypotheses as well as simulation of rocks based on any conceivable combination of them. The benefits of a unifying scheme for description of crystalline parent rocks and their weathering products are illustrated by exploratory analysis of a petrographic data set derived from five granodiorites from across North America, comprising the parent rocks and three size fractions (coarse, medium, and fine) of their detritus. Compositional data analysis is used to estimate sediment generation and evolution (SGE) trajectories for each of the plutons sampled. The bulk mineral composition and the mineral composition of the rock-fragment assemblage display a common trend of relative depletion of quartz and K-feldspar with decreasing grain size, compensated for by relative enrichment of biotite and accessory minerals. The evolution of crystal interface composition suggests that the balance between chemical and mechanical weathering may be reflected in relative stabilities of crystal interfaces. We propose a computationally efficient stereological inversion procedure for estimating the parameters of crystal-size probability distributions in rocks based on the assumption of log-normality. The lognormal distribution is an acceptable default model for crystal size in granitoids at the level of individual thin sections (about 87% passes the tests for lognormality), but less so at the level of entire plutons (only 62% success ratio). The current implementation of the GGD is not yet complete, because it deals explicitly with the first three fundamental properties only, as a consequence of adopting the simplifying assumption that all elements which make up a rock are spherical. Shape and orientation distributions may be included in future implementations of the GGD. Dedicated data sets comprising sediments generated from a single parent rock under different conditions will be needed to advance SGE studies by shedding more light on the balance between chemical and mechanical weathering.

The definition of a rock as an aggregate of minerals is equivalent to defining a population as an assemblage of elements (Griffiths, 1961).

1. Introduction

The primary controls on the type of sediment released from source areas are the mineralogical composition, texture, and crystal or particle

size of the parent rocks (Johnsson, 1993; Heins, 1995; Basu, 2003; Weltje and von Eynatten, 2004; Weltje, 2012; Allen, 2017, p. 301). Sediments that enter the fluvial transport system are likely to display certain characteristics inherited from their parents and the regolith from which they were derived (e.g., Nesbitt, 2003; Caracciolo et al., 2012). On their way to the sink, sediments are subjected to a range of selective modifications that contribute to the evolution of their properties. The extent of modification depends on a range of factors that are

* Corresponding author.

E-mail address: bram.paredis@kuleuven.be (B. Paredis).

commonly grouped under climatic (e.g., Basu, 1985; Suttner and Dutta, 1986) and tectonic regimes (e.g., Dickinson, 1985). Extreme cases of modification have been documented from large drainage basins in low-relief humid tropical settings, such as the Amazon and Orinoco basins, where residence times are long, chemical weathering is dominant, and the properties of detritus supplied to the coast deviate sharply from those of the starting material (Potter, 1986; Johnsson et al., 1988; Johnsson et al., 1991). The other extreme is represented by detritus produced under conditions fully dominated by mechanical weathering, where residence times are short and/or rates of chemical weathering are slow owing to the absence of water (Ibbeken and Schleyer, 1991; Nesbitt and Young, 1996). But even in the latter case, the petrographic composition of detritus varies with size (Caracciolo et al., 2012; von Eynatten et al., 2012). Quantitative description of this spectrum of modifications must be built on integrated data sets that permit analysis of the co-evolution of multiple sediment properties, starting from the properties of their parents.

Quantification of the initial properties of sediments and their modifications in transit is one of the fundamental tasks of sedimentary petrology. Analysis of sediment generation and evolution (SGE) seeks to capture changes to the detrital spectrum of sediments in response to selective modifications along the pathway from source to sink. The prevailing approach to reconstructing the conditions in source areas of sediments has been based on analysis of their properties (Dickinson, 1985; Suttner and Dutta, 1986; Johnsson, 1993; Basu, 2003; Weltje and von Eynatten, 2004). The complementary approach is to predict sediment properties based on the conditions under which sediments have been formed. Methods for prediction of sediment properties are still in their infancy, but several studies have outlined their potential (Ibbeken and Schleyer, 1991; Heins and Kairo, 2007; Weltje, 2012; Weltje et al., 2018).

A prerequisite for achieving rigorous quantification in SGE studies is a solid descriptive framework capable of capturing the textural and compositional properties of parent materials and their weathering products with the same set of parameters, to permit direct comparisons and analysis of genetic relations among them. The foundations for such a comprehensive descriptive framework were presented by Griffiths (1952, 1961) and form the backbone of his monograph on the analysis of sediments according to the scientific method (Griffiths, 1967). Griffiths (1952, 1961, 1967) developed his description of the aggregate properties of rocks with sediments in mind, but the concept underlying it is of broad significance to petrology in general. In this contribution, we will present an extension of his scheme, which we termed the Generalized Griffiths Descriptor (GGD). The GGD lends itself to the description of a wide range of rock types, and therefore, may be used to describe and analyse full SGE trajectories in compositional-textural space. The starting point of each trajectory represents the fundamental properties of the parent rocks of sediments (Weltje et al., 2018). Specification of fundamental properties permits us to illustrate the power of the GGD by showing how joint analysis of igneous rocks and their weathering products in an appropriate statistical framework leads to new insights into the nature of SGE trajectories.

2. The conceptual model of Griffiths

2.1. Fundamental properties

The number of properties one could measure with the objective to characterize an arbitrary specimen of rock or sediment is potentially infinite. In order to decide which properties permit complete characterization of a specimen in the most efficient way, their information content has to be taken into account. The smallest number of variables needed for a complete description of an aggregate is obtained when all variables are statistically independent and contain only unique information. Griffiths (1961) used this idea to identify the fundamental properties of an aggregate. The fundamental properties must contain all

information needed to define uniquely a specimen, subject to the constraint that their number must not be larger than needed for the unique definition of the specimen. In formal statistical terminology, these two requirements are known as *sufficiency* and *necessity*, respectively.

The five fundamental properties identified by Griffiths (1961) are defined in terms of the elements (petrographic classes) of an aggregate. They are: (1) kinds and volumetric proportions of the elements; (2) spatial arrangement ("packing") of the elements; (3) size distributions of the elements; (4) shape distributions of the elements; and (5) orientation distributions of the elements. "With regard to the question why these particular properties should be chosen, the answer is that these properties suffice to encompass a set of objects in a very wide range of fields of endeavour; thus a mineral is made up of atoms of certain kinds, in certain proportions, and of certain sizes, shapes, and arrangements (orientation and packing); again, the universe is composed of stars of certain kinds, in certain proportions, of certain sizes, shapes, and positions; finally, an element such as sodium is composed of electrons, protons, etc., of certain sizes, shapes, and arrangements. It is contended therefore that this set of five properties is a fundamental set which, upon precise specification, will lead to the unique definition of an aggregate of elements at any level, i.e., specification of these properties fulfils the necessary and sufficient conditions for a unique description of the aggregate" (Griffiths, 1961).

The concept of statistical independence of the five fundamental aggregate properties may be illustrated by the following thought experiment. Suppose that person A has access to an aggregate and is in possession of the full knowledge about all of its fundamental properties. Person A is willing to share all possible information about one of its fundamental properties with person B, who does not have access to the aggregate. If person A would ask person B: "What can you say, based on the exhaustive information I have shared with you on this fundamental property, about any of the other four fundamental properties of the aggregate?", the invariable answer of person B would be: "Nothing."

The existence of an exhaustive set of statistically independent fundamental properties implies that: (1) all other properties (so-called derived properties in the terminology of Griffiths (1961)) reflect some form of interaction among fundamental properties and can be predicted if the fundamental properties are known, and (2) any statistically significant interrelationship among fundamental properties (either on the level of a single specimen or on the level of a lithosome) must reflect non-random petrogenetic processes (Griffiths, 1952, 1961).

Petrogenetic inference from fundamental properties is illustrated by analysis of the joint size-shape distributions of sediments. Operational definitions of grain shape in sediments are statistically independent of the sizes of grains (e.g., Barrett, 1980; Diepenbroek et al., 1992; Blott and Pye, 2008), which implies that there is no intrinsic statistical reason for correlation between shape and size. Hence, the fact that grain size and shape in natural sediments are correlated (Curry and Griffiths, 1955; McEwen et al., 1959; Moss, 1966; Youd, 1973) must reflect some combination of petrogenetic factors, i.e., provenance (parent lithology), selective modification (chemical and mechanical weathering), and selective transport (aerodynamic or hydraulic sorting according to size, shape, and density).

The starting point of Griffiths (1952, 1961) was to focus on the smallest set of properties needed to arrive at a complete petrographic description at the scale of thin sections, without explicit reference to data-acquisition technology. The theory of Griffiths refers only to the properties one wishes to describe and not to the variables which are being measured according to analytical protocols. The continuous development of data-acquisition technology likely is to be reflected in the evolution of workflows for characterization of rocks and sediments. It is conceivable that multiple combinations of measurement techniques may be able to capture fundamental rock properties. Conversely, some fundamental properties may be difficult to isolate based on measurements. The current practice of trying to infer fundamental properties of rocks from measurements on plane and thin sections is a case in point.

Cuts through a specimen reveal an assemblage of elements whose apparent (2-D) properties result from some interaction of particle/crystal size, shape, and orientation. If these three fundamental properties were known (and the relations among them were fully specified), one could predict the corresponding 2-D properties as observed on a specimen of finite size in a statistical sense. Unfortunately, the opposite does not hold: the 2-D observations of apparent size, shape, and orientation contain insufficient information to provide a unique estimate of the three fundamental properties. Stereological inversion of the size distributions of elements from 2-D measurements is therefore carried out by making assumptions about the way in which shape and orientation of grains depend on their (apparent) size. Hence, the statistical independence of fundamental properties does not imply that we can or, for that matter, should be able to measure them independently.

2.2. Elements of the population

Griffiths (1961) stated that the definition of a specimen of rock as an aggregate of minerals is equivalent to defining a population as an assemblage of elements. The definition of elements merits some discussion, as Griffiths (1961) referred to the petrographic analysis of sand and sandstone only, and did not explicitly distinguish between mono- and polymimetic grains. Our objective is to extend his concepts to metamorphic and igneous rocks by adaptation and generalization of sediment-petrographic criteria.

The choice of a petrographic classification scheme is logical because it is grain-based: it would not make much sense to describe the composition of sediment that consists primarily of polymimetic grains in terms of its constituent minerals alone. The grains are the natural units of observation because their properties (size, shape, and density) determine how the sediment will be transported and fractionated on its way from the source to the sink. A petrographic description of sediments that includes information on the mineralogical composition of the polycrystalline grains may be used to predict the bulk mineralogical composition of specimens. In contrast, it is not possible to predict the petrographic composition of a specimen from its mineralogical composition in the absence of additional information (grain and crystal sizes, interface frequencies) and therefore it may be concluded that the petrographic description contains more information than the mineralogical description.

It follows logically from the above that trying to understand the behaviour of sediments based on their bulk mineral composition instead of their petrographic composition would be much harder, in view of the fact that the physical properties of the individual minerals (i.e., their sizes, shapes, and densities) do not directly govern the behaviour of the sediment, even though it seems likely that they must be related to it in an indirect way. This problem is amplified in the case of geochemical characterization, which is currently the most popular method for describing the composition of rocks and sediments with a common set of variables. Here, the term elements as used by Griffiths (1961) can be taken literally. Again, it is much easier to predict bulk chemical composition from a petrographic or mineralogical description than to do the opposite. Because chemical composition is defined in terms of the lowest common denominator of rocks and sediments it may even be difficult to predict whether a bulk chemical composition refers to a sedimentary, metamorphic, or igneous rock in the absence of additional information. Another potential problem is that of compositional collinearity (Harvey and Lovell, 1992), which arises from the fact that there are many more minerals than chemical elements. Collinearity occurs whenever several minerals have the same chemical composition (polymorphs) or the chemical composition of one or more minerals can be expressed as a mixture of other minerals present in the specimen (solid solutions). In such cases, there is no unique mineral composition for a given chemical composition. The link between chemical composition and fundamental properties of sediments is indirect at best, as the behaviour of chemical elements depends on the mineral phase in which

they are present, and the behaviour of the minerals, in turn, reflects the properties of the monocrystalline grains of that mineral class, as well as the properties of any polycrystalline grains in which they occur.

Characterization of rocks on the three levels discussed above (chemical, mineralogical, and petrographic) may be placed in the compositional hierarchy applicable to SGE studies (Weltje, 2012). Conceptually, the levels in this hierarchy are defined by mixing. Minerals are mixtures of chemical elements, grains are mixtures of minerals, and grain assemblages are mixtures of grains supplied by different sources and/or mechanisms. In principle, each of these levels could be taken as a reference to define the elements which make up a rock. In practice, the choice of level is guided by the trade-off between the efficiency of data acquisition on the one hand, and the desired level of petrological characterization on the other hand. Geochemical analysis is easily automated but gives low-level information, whereas petrographic analysis may be time-consuming but returns high-level petrological information.

2.3. The target population

Griffiths (1961) considered two approaches to exhaustive characterization of an aggregate: (1) The object-based approach, in which the class, spatial coordinates, size, shape, and orientation of each object (element) are specified to uniquely define the aggregate; (2) The statistical approach, in which each of the five properties is described as a probability distribution applicable to the aggregate as a whole. The petrographic description of aggregates according to the model of Griffiths pertains to a single specimen at the scale of a thin section or its equivalent volume, as sampled by digital image analysis, micro-CT scanning, chemical analysis (ICP, XRF), and petrographic modal analysis. Progress in data-acquisition technology (micro-CT, dynamic and static image analysis) has brought the 3-D object-based approach within reach. But even if object-based measurement of all five fundamental properties of a specimen is possible, there is still the issue of upscaling to consider, because the target population of rock-characterization exercises is usually not the thin section, but the rock body as a whole. As discussed above, it is possible to examine whether or not size and shape of sediment grains are correlated based on analysis of a single specimen, but we cannot extrapolate this knowledge to predict the spatial variability of grain shape within a higher-level target population such as an entire lithosome from the knowledge of bulk grain size alone. Because fractionation of grains is governed by combinations of size, shape, and density, we would need information on the other properties (in this case, modal composition and particle-size distributions of each modal class). In many cases, several competing explanations exist of the dominant controls on spatial variability of properties within a chronostratigraphically constrained lithosome (or chronosome sensu Schultz, 1982) of a sedimentary basin fill. The spatial variability of properties within the chronosome may reflect mixing of sediments from multiple sources, the net effect of selective sediment dispersal, or (most commonly) some combination of both, as illustrated by Weltje and Brommer (2011). Each of these potential explanations implies different covariances among the set of fundamental properties. Geospatial modelling of fundamental properties across entire lithosomes is discussed in more detail in a companion paper (Weltje and Paredis, this issue).

3. The Generalized Griffiths Descriptor (GGD)

The GGD may be used to describe the fundamental properties listed above to encompass a wide range of rock types, i.e., sedimentary, metamorphic, and igneous rocks. Each of the properties of the GGD represents a multivariate entity (i.e., a probability distribution or its discretized equivalent, a vector or matrix). In implementing the GGD, we will keep things as simple as possible, reflecting the current state of the art in sediment characterization. Fig. 1 illustrates the data-acquisition protocol used to estimate the first three fundamental properties.

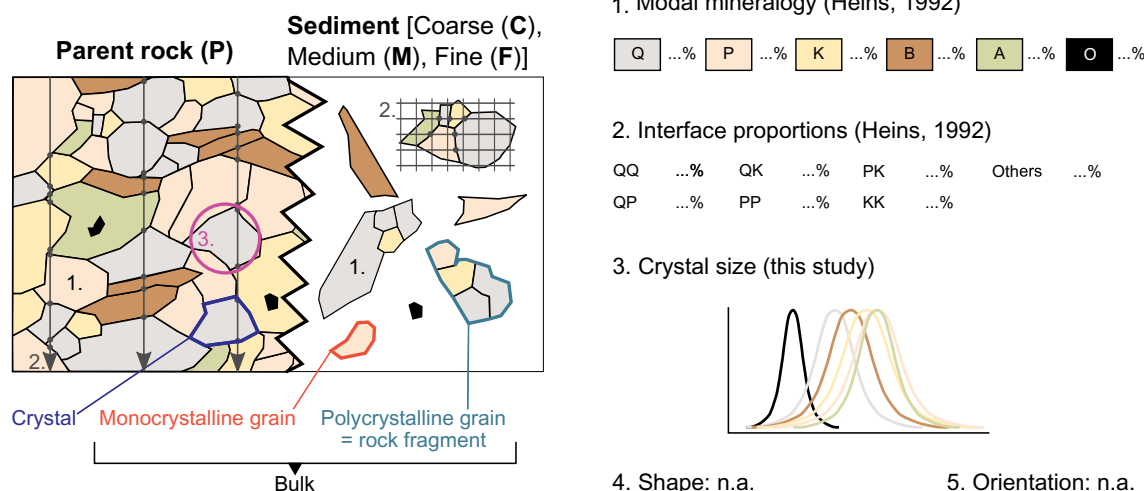


Fig. 1. Schematic thin-section representation of parent rocks and sediments to illustrate acquisition protocol used for estimation of the first three fundamental properties (as well as data sources). Property 1, the modal composition, is based on 500 (P) or 300 (C, M, F) point counted per thin section. Property 2 corresponds to several thousand tallies of crystal interfaces along linear traverses predefined by the operator (P) or along lines defined by an ocular grid (C, M, F). Property 3 is defined for the parent rock only. It is related to the size distribution of the equivalent circular diameter (D) of a number of selected crystals (n) belonging to a given mineral phase. Properties 4 and 5 have not been measured.

3.1. Modal composition (property 1)

The modal composition represents the volumetric proportions of the elements of the population. It is represented by a vector with m elements. For point-count data, let $x_{j|}$ be the number of points falling on element j . Then, the modal proportion $\langle x_j \rangle = x_j/X$, where X is the total number of points.

The elements of the population refer to petrographic classes. Petrographic classes are categorical data, which fulfil two criteria: (1) the classification scheme must be exhaustive, and (2) its classes (categories) must be mutually exclusive. These two requirements permit each element to be uniquely assigned to a category. In practice, this leads to the definition of an ‘Others’ group comprising all other minerals than those specifically named, for instance, several species of comparatively rare accessory minerals. Operational definitions of petrographic classes in sandstones include various categories of mono- and polycrystalline framework grains and any other phases (i.e., different types of matrix, cement, and voids). In igneous rocks such as granites and metamorphic rocks such as gneiss and schist, petrographic classes correspond to interlocking crystals. In porphyritic rocks, consisting of phenocrysts in a cryptocrystalline groundmass, not all mineral phases can be resolved individually, and a category termed groundmass may be defined, analogous to the matrix of sandstones.

Measurement of modal composition is generally straightforward, either directly (point counting, digital image analysis) or by proxy (XRD combined with chemical analysis). As discussed above, bulk chemical composition may be upgraded to bulk mineral composition if the chemical compositions of all minerals are known, and there is no collinearity of mineral composition (polymorphs and solid solutions). Mineral compositions of sediments cannot be routinely converted to petrographic composition in the absence of textural information.

3.2. Spatial arrangement (property 2)

If it is assumed that the spatial arrangement of elements is random (as in detrital sediments), it may be fully described by a single dimensionless number known as the packing density (Kahn, 1956). The packing density is defined as the product of the number of grain-to-grain contacts in a linear traverse of a thin section, and the average intercept size of the grains, divided by the total length of the traverse. The packing density of framework elements is independent of mineral

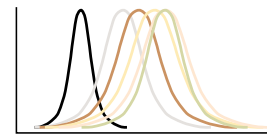
1. Modal mineralogy (Heins, 1992)

Q ...%	P ...%	K ...%	B ...%	A ...%	O ...%
--------	--------	--------	--------	--------	--------

2. Interface proportions (Heins, 1992)

QQ ...%	QK ...%	PK ...%	Others ...%
QP ...%	PP ...%	KK ...%	

3. Crystal size (this study)



4. Shape: n.a.

5. Orientation: n.a.

composition and average size. Its complement (i.e., one minus the packing density) is also known as the intergranular volume (IGV) fraction (Paxton et al., 2002).

Generalization of the above measure to rocks that display non-random textures is needed to extend the original scheme of Griffiths (1961) to metamorphic and igneous rocks. A multivariate measure of spatial arrangement in the form of interface frequencies (1-D) was proposed by Weltje et al. (2018), based on the work of Vistelius (1972) and Aitchison (1986). With this measure, three types of texture can be distinguished: ordered, random, and clustered (Jerram et al., 1996; Weltje et al., 2018). In this scheme, random texture marks the midpoint between ordered and clustered texture. In essentially isotropic rocks such as granitoids, which tend to display ordered texture, interface frequencies are independent of the orientation and direction of a linear traverse through a thin section (Sharp and Severance, 1991). In anisotropic rocks such as laminated sediments or foliated metasedimentary rocks, the spatial arrangement should be measured perpendicular to the main direction of the lamination/foliation; such rocks will display clustered texture. Random texture is expected to occur in detrital sediments which are homogeneous on the scale of a thin section.

The interface frequencies in a rock comprising m elements can be summarized by a vector with $k = m(m + 1)/2$ classes. Observed interface frequencies depend on the number-frequency distribution of elements in an aggregate, and this effect must be removed to obtain a description of spatial arrangement that fulfils the criteria of a fundamental property. The fundamental property that may be derived from interface frequencies is termed the *interface composition*. It captures the abundance of crystal interfaces in a rock, normalized to the abundance of expected interfaces in a rock with exactly the same number-frequency distribution of elements, but possessing random texture.

Let f_i denote the observed frequencies. The total number of observed interfaces $F = \sum_{i=1}^k f_i$, and the interface proportions are defined as: $\langle f_i \rangle = f_i/F$. Note that non-isomineralic interface proportions between minerals A and B are defined as the sum of transitions from A to B and those from B to A .

Number frequencies of the elements (n_j) may be calculated from the set of k interface counts (f_i) as shown by Weltje et al. (2018) and in Appendix A. Alternately, they can be obtained by summing the elements of the $(m \times m)$ matrix of observed transitions, either row- or column-wise. The total number of elements encountered is equal

$toN = \sum_{j=1}^m n_j$, and the number proportions are given by: $\langle n_j \rangle = n_j/N$.

Expected frequencies (\hat{f}_i) under the assumption of random texture may be calculated from the number-frequency distribution of elements as follows (Weltje et al., 2018). The law of independent events specifies that in case of random texture (here illustrated for two elements A and B), the expected interface proportions (transition probabilities) are directly related to the observed number proportions of elements: $\langle \hat{f}_{AA} \rangle = \langle n_A \rangle^2$, $\langle \hat{f}_{BB} \rangle = \langle n_B \rangle^2$, $\langle \hat{f}_{AB} \rangle = 2\langle n_A \rangle \langle n_B \rangle$. Absolute predicted interface frequencies are obtained by multiplication: $\hat{f}_i = F(\hat{f}_i)$. The interface composition is defined as the vector α consisting of k elements, given by $\alpha_i = f_i/\hat{f}_i = \langle f_i \rangle / \langle \hat{f}_i \rangle$. Random texture is represented by $\alpha = 1$.

It may be noted that the direction of a fabric-perpendicular traverse is not likely to be of interest to the description of foliated metasedimentary rocks but will prove to be essential in the case of sediments with asymmetric (fining or coarsening up) laminae. We propose that such sediments be traversed “bottom-up” in accordance with the stratigraphic facing direction. Moreover, asymmetric spatial arrangements cannot be described by a single vector, but require the raw transect data of observed transitions from which higher-order Markov chain models (Vistelius, 1972; Whitten and Dacey, 1975; Sharp and Severance, 1991) or other multivariate time-series representations such as auto-covariance functions (Morishita and Obata, 1995; Morishita, 1998) may be derived. Capturing the spatial arrangement of elements in 2-D is considerably more complex than in 1-D, as the observed lengths of interfaces in thin or plane section are related to apparent element sizes (property 3) and shapes (property 4) as well (Caracciolo et al., 2012). The 1-D interface composition as defined above is an adequate tool for characterizing the spatial arrangement of petrographic classes within a specimen at the current level of SGE studies, and its operational definition (counting of crystal interfaces in linear transects) is straightforward.

3.3. Size-frequency distributions (property 3)

This property may be represented by m continuous distribution functions, or in discrete form as a $[m \times b]$ matrix, where b is an arbitrary number equal to the number of size bins. Alternatively, it may be specified by the parameters of a class of probability distributions (log-normal, log-linear, etc.)

Property 3 pertains to the size-frequency distributions of the elements (petrographic classes) in the form of probability distributions (relative frequencies summing to unity). In sedimentary petrology, specification of the size-frequency distribution of each class of elements separately has proved to be essential for understanding the relation between size and density of mineral grains in wind and water-sorted sediments (Schroeder van der Kolk, 1898; Rubey, 1933).

The bulk grain-size distribution (GSD) as commonly employed in sedimentary petrology is not equivalent to property 3, because the GSD is not a particle size-frequency distribution, but a particle mass-frequency (e.g., sieving) or volume-frequency (e.g., laser diffraction) distribution. Other measurement techniques (e.g., Sedigraph) record a fall-velocity distribution. The implicit assumption in all these techniques is that particles are spherical. In general, no technique measures all particle properties (i.e., size, shape, and density) simultaneously. Conversion from mass- or volume-frequency distributions to number frequency distributions is thus not exactly trivial. A promising approach for unconsolidated sediments is dynamic image analysis (DIA), which permits capturing of individual particles with high-speed cameras, and is able to provide joint size-shape frequency distributions as output (combination of properties 3 and 4). If DIA protocols could be extended to measure terminal settling velocities of particles, one could solve for particle density (using the equation of Wu and Wang (2006)) so as to obtain a proxy of modal composition (property 1).

The crystal-size distribution (CSD) as defined in igneous and metamorphic petrology (Marsh, 1988; Higgins, 2006b) is a number-frequency distribution, but it is not a probability distribution, and therefore it does not fulfil the requirements of a fundamental property. The CSD is expressed in terms of absolute numbers of crystals of a given size per unit volume, and thus simultaneously acts as a measure of the modal composition (property 1). Examples of the interplay between the CSD and modal composition may be found in Fig. 1 of Higgins (2002). Accurate conversion from CSDs to modal composition requires information on grain shape (property 4) (Higgins, 2002).

The CSD is not suitable for examining inter-relations between fundamental properties because it is actually a measure which contains information on three of them (properties 1, 2, and 4). In order to permit testing of the hypothesis that modal composition varies independently of the size distributions of crystals, the intrinsic link between crystal size and modal composition must be broken by expressing the CSD of element j as a probability density function $g_j(D)$, in which the cumulative probability distribution of crystal sizes is expressed as $\int_0^\infty g_j(D) \delta D = 1$, in accordance with general practice in mathematical statistics (Weltje et al., 2018). Strictly speaking, the term CSD should be applied to such “normalized” probability distributions only, which have been decoupled from the modal composition. For the sake of clarity, we will refer to fundamental property 3 as the *crystal-size probability distribution* (CSPD).

CSPDs cannot be directly observed in plane or thin sections, because these only provide information on the size distributions of 2-D cross-sections of elements. The statistical techniques developed to estimate 3-D distributions from distributions of lower dimensionality belong to the field of stereology. Methods of stereological inversion of crystal-size data obtained from thin or plane sections have been frequently applied in petrology (Peterson, 1996; Sahagian and Proussevitch, 1998; Higgins, 2000; Armienti and Tarquini, 2002; Berger et al., 2011). Inversion is usually carried out under the assumption that a characteristic shape (property 4) can be assigned to each class of elements, i.e., the possible dependence of shape on size is not taken into account. The estimated 3-D distributions are strongly affected by the shape factor adopted. This is partly the result of the fact that the CSD as defined in petrology also contains information on the modal composition, but it is also an inherent limitation of all techniques which assume a fixed shape across the full range of element sizes. A more flexible model in which also the relation between size and shape of the elements is considered was proposed by Cruz Orive (1976, 1978). This method may be applied to inversion of ellipses assumed to represent random cuts through populations of either prolate or oblate ellipsoids with variable axial ratios. For more complex shapes such as triaxial ellipsoids, a unique solution does not exist. Note that random cuts carry the assumption that the orientation of the elements (property 5) is random as well.

Despite the likely inter-relationship among size, shape and orientation distributions (properties 3 to 5) in geological populations, remarkably good results have been obtained with parametric fitting of spherical particle distributions to 2-D data (Proussevitch et al., 2007a, 2007b; Jutzeler et al., 2012). In these studies, the quality of stereological estimates was assessed relative to the results of sieve analyses on the same set of specimens. The lognormal distribution was shown to provide the best estimates relative to the other classes of distributions functions considered (Jutzeler et al., 2012).

In the petrological literature, the log-linear distribution is commonly adopted as the reference model (Marsh, 1988; Higgins, 2006b). By definition, data following a log-linear distribution form a straight line on a plot of the logarithm of population density against size. But even if the 3-D data would follow a reference model such as the log-linear distribution, one cannot expect the inverted data to plot exactly on a straight line owing to truncation effects (see Fig. A1). Crystal size data show truncation in the fine tail of the distribution (left-hand truncation) towards the lower limit of resolution of the adopted

measurement technique. The coarse tail of the distribution is affected by right-hand truncation because elements will not be counted unless they fall entirely within the specimen, i.e., partial grains at the edges of the specimen are not counted. The larger the elements, the higher the probability that they will intersect one of the edges of the specimen, and the upper size limit of elements that can be measured is by definition equal to the smallest dimensions of the specimen (under the assumption of spherical grains). Under-representation of the largest and smallest crystal elements must be taken into account before attempting any interpretation of CSPDs (Armienti and Tarquini, 2002).

It is fairly straightforward to apply stochastic simulation techniques to generate unique 2-D data sets from any fully specified 3-D population (joint size-shape-orientation distributions), as shown by Burger and Skala (1976) and Harvey and Ferguson (1978). By contrast, the inverse approach is fraught with difficulty and a unique 3-D solution to an arbitrary set of observed 2-D data does not exist. Each 3-D solution should, therefore, be viewed as an approximation, whose quality is determined by the parameters of the data-acquisition scheme (dimension of the specimen, lower limit of resolution, number of elements counted) and the reasonableness of assumptions with regard to the relations among size, shape, and orientation of the elements (properties 3 to 5). An additional boundary condition is the amount of time and effort one is willing or able to spend on the estimation of crystal-size probability distributions in view of the purpose of the investigation. Details of the CSD are considered to be highly relevant in the field of petrology because they are commonly interpreted in terms of petrogenetic mechanisms (e.g., nucleation and coarsening). In the case of characterizing parent rocks for the purpose of SGE studies, a first-order approximation based on simplifying assumptions is considered sufficient, as sediments generated in first-order drainage basins are comprised of mixtures of material derived from spatially heterogeneous parent rocks. Appendix A contains the procedure for estimating CSPDs adopted in this study.

3.4. Shape and orientation distributions (properties 4 and 5)

These properties may be represented by m continuous distribution functions, or in discrete form as a $[m \times b]$ matrix, where b is an arbitrary number equal to the number of shape or orientation bins.

Most of our knowledge about shape and orientation stems from the analysis of thin sections, which provides 2-D measures in the form of apparent size and shape only (Chayes, 1956; Griffiths, 1967). Such 2-D measures may be converted to 3-D properties under various assumptions (Cruz Orive, 1976, 1978; Higgins, 2000). Shape analysis of crystals in 3-D may be carried out by serial sectioning (e.g., Marschallinger, 2001) or tomography (e.g., Robin and Charles, 2015).

In crystalline rocks, a distinction between crystal (or lattice) preferred orientation (CPO) and shape preferred orientation (SPO) is made (Higgins, 2006a). The latter seems to be the most valid for SGE studies since it deals with the orientation of the outlines of the crystals (or grains in the case of sediments). For obtaining the SPO of individual crystals/grains in 3-D, electron backscatter diffraction (EBSD; e.g., Kilian et al., 2011, Kahl et al., 2017), serial sectioning (e.g., Marschallinger, 2001), or micro-computer tomography (micro-CT) (e.g., Schöpa et al., 2015; Kahl et al., 2017) may be used. Optical microscopy of thin sections with a universal stage can also provide information on 3-D CPO. For a detailed overview of other methods to obtain information on shape and orientation, see Higgins (2006a).

Micro-CT scanning could be used to image rock specimens of up to 1 cm^3 in 3-D at a sufficiently high spatial resolution to resolve their elements through the identification of discrete phases, which would have to be followed by segmentation into grains in the case of sediments. Unfortunately, the distinction of quartz from feldspars cannot be reliably achieved with this technique (Long et al., 2009), which renders it unsuitable for petrographic analysis of sandstones. This problem stems from the nearly identical attenuation coefficients of quartz and

feldspars (a function of their mean atomic number and packing density). Separation of quartz into detrital components (grains) and authigenic components (overgrowths) is likewise impossible with this technique. Segmentation among classes of elements with distinct attenuation coefficients with micro-CT is thus likely to produce fewer than m groups. Some of these groups will comprise multiple petrographic classes, which may be undesirable given the required level of detail in the definition of property 1. Given the problems associated with segmentation, a pragmatic solution is to extract a single joint size-shape-orientation distribution from micro-CT data which summarizes all elements in the aggregate.

The shapes and orientations of non-framework elements of sedimentary rocks (matrix, pores, cement) are fully defined by their complement, the framework elements surrounding them. The same would apply to the groundmass of porphyritic rocks (broadly equivalent to the matrix of sedimentary rocks), and even to the shape of quartz in granitoids, as quartz is commonly the last phase to crystallize and its apparently random spatial distribution seems to indicate that it simply fills any remaining space (Weltje et al., 2018).

In our application of the GGD to the set of parent rocks and derived sediments presented below (for which no information on shape and orientation distributions is available), we will adopt the simplifying assumption that all elements (crystals/grains/non-framework classes) are spherical. This eliminates properties 4 and 5 from the GGD. While this assumption may be regarded as an oversimplification, for instance when applied to the shapes of micas or overgrowths on detrital grains, it should be borne in mind that it is not yet possible to routinely measure all fundamental properties of rocks, and the simplification achieved by eliminating properties 4 and 5 from our current implementation of the GGD is considered a necessity at the present level of description. It also permits a straightforward transformation of the bulk GSD as defined in sedimentary petrology to a size-frequency distribution (property 3) under the additional assumption that the range of grain densities is limited and does not correlate with size.

Recently, Graham and Gadsden (2019) formulated a rigorous statistical framework for the analysis of shape distributions as ternary compositions, whose values are functions of the long, intermediate, and short axes of reference ellipsoids. Suitable classes of orientation distributions (spherical data) have been described by Fisher et al. (1987). These and similar references may be used to develop precise operational definitions of properties 4 and 5 needed to adequately summarize these aggregate properties.

3.5. Internal consistency of the GGD

Owing to the statistical independence of fundamental aggregate properties, it is possible to describe rocks that display any conceivable combination of fundamental properties in an internally consistent manner. Below we discuss the inverse of this approach, i.e., simulation of any conceivable rock from a randomly chosen set of fundamental properties.

The size-frequency distribution of element j , $g_j(D)$ permits calculation of the arithmetic mean volume of the element under the assumption that its shape is known (Higgins, 2002). For spherical elements:

$$\bar{v}_j = \frac{\pi}{6} \int_0^\infty g_j(D) D^3 \delta D$$

With the help of the arithmetic mean element volume \bar{v}_j we can simulate any given volume of rock based on the first three fundamental properties of the GGD. In any fixed volume of rock (V_R), the following must hold:

$$n_j = \frac{V_R x_j}{\bar{v}_j}$$

Hence, the total number of elements of class j (n_j) in the volume of

Table 1

Description of plutons and sample sizes of Heins (1992) used in this study.

Pluton	Granite Wash Mountains	Kinney Lakes Granodiorite	Kinney Lakes Granodiorite	Ocotito Granitoid Complex	McCartney Mountain Stock	Mt. Stuart Batholith
Location	West-central Arizona, USA	Sierra Nevada, California, USA	Sierra Nevada, California, USA	Sierra Madre del Sur, Guerrero, Mexico	Southwestern Montana, USA	Cascades, Washington, USA
Coordinates	33.708 N, 113.639 W	38.568 N, 119.852 W	38.568 N, 119.852 W	17.148 N, 99.541 W	45.508 N, 112.647 W	47.479 N, 120.805 W
Code	AZ	CA-EW	CA-NS	GR	MT	WA
# samples	P 15 C, M, F 8	6 9	5 10	10 6	8 8	4 6
Mean interface counts	P 7142 C 3571 M 1315 F 957	2962 1216 369	2426 1168 404 417	4856 1069 758 588	5044 1447 575 592	4067 1195 449 538

rock to be simulated can be calculated given the modal proportion of that element (x_i) and its arithmetic mean element volume \bar{v}_i . The above equation shows that the number-frequency distribution of the elements (n_i) is derived from the combination of volumetric proportions (property 1) and average volumes (property 3) of the elements, and is thus not a fundamental property. However, it does fulfil an essential role, because it is also related to the components of the interface composition α_i (property 2), and can be used to retrieve the actual interface proportions in the volume of rock to be simulated. The predicted interface proportions $\langle \hat{f}_i \rangle$ under the assumption of random texture may be derived from the number-distributions of the elements $\langle n_i \rangle$ as explained in the section on property 2. The actual interface proportions of the rock to be simulated are given by:

$$\langle f_i \rangle = \frac{\langle \hat{f}_i \rangle \alpha_i}{\sum_{i=1}^k \langle \hat{f}_i \rangle \alpha_i}.$$

It is thus always possible to generate an internally consistent hypothetical rock from a random combination of modal composition, interface frequencies, and crystal-size probability distributions. This is an important prerequisite for 3-D simulations of rocks which honour the above three constraints simultaneously (cf. Burger and Skala, 1976; Harvey and Ferguson, 1978). Explicit geometric composition-texture models in 2-D have been proposed by Wang (2015), Van der Wielen and Rollinson (2016), and McCanta et al. (2017), whereas 3-D models have been proposed by Elsey et al. (2011), Miyoshi et al. (2017), and Hilden and Powell (2017). The extent to which crystal-size distributions and non-random spatial distribution patterns of crystals are accommodated differs among the above models. As yet, no model permits direct incorporation of interface-frequency data to constrain the spatial distribution of elements. Similar limitations apply to the specification of shape and orientation distributions of the elements (properties 4 and 5). Considerable model development is needed to permit accurate simulation of the joint compositional-textural variability of rock specimens as observed in thin section.

4. Material and methods

4.1. Material

Heins (1992, 1993, 1995) sampled five subaluminous granodiorite plutons and their sediments in the Cordillera of the United States and Mexico. Sand was collected from first-order drainages developed directly on fine- to medium-grained, equigranular phases of plutons to minimize parent-rock variation.

Direct comparison between parent rocks and sediments based on petrographic criteria is not very meaningful (from a petrographic point of view, a parent rock represents a single “rock fragment” of near-infinite size), so instead, the mineral composition was used for comparative purposes. Each sample was characterized in terms of modal

mineralogy (property 1) and crystal-interface frequencies (property 2). The data set of one pluton (CA) was considered large enough to be subdivided into two groups according to the orientation of the drainage (E-W and N-S). The sediment data set comprises analyses of three size fractions (coarse, medium, and fine), in which the mineral composition of the monocrystalline grains and that of the polycrystalline grains (rock fragments) were tallied separately. These separate tallies give rise to two variants of property 1, termed 1a (bulk mineral composition) and 1b (mineral composition of the rock-fragment assemblage), respectively. The data-acquisition protocols and operational definitions used have been outlined in full detail in Heins (1992, 1993, 1995) and Weltje et al. (2018). The original thin sections of the parent rocks (Heins, 1992) were revisited to estimate crystal-size probability distributions of the minerals in each pluton (property 3). Fig. 1 illustrates the data-acquisition scheme adopted for the estimation of the first three properties. An overview of the data set is presented in Table 1 (the full data set is provided as online supplement).

4.2. Crystal size probability distributions

The only information on the CSPDs of minerals in the parent rocks (property 3) is given by the arithmetic averages of the lengths of crystal intercepts (1-D apparent diameter) obtained from the parent-rock interface tallies of Heins (1992). Therefore, the original thin sections of the parent rocks were revisited to estimate crystal-size distributions of the minerals in each pluton. The thin sections were digitized by taking ca. 200 pictures per thin section in circularly polarized light (CPL) (Higgins, 2010). The pictures were stitched together using the software package PTGui. CPL is very useful for the purpose of tracing crystal boundaries. It highlights texture because all crystals will show their maximum birefringence colour for their respective cross-section independently of their orientation with regard to the polarizers. This allows identification of the majority of crystals from the images without the need for a microscope. Flatbed scan images of the thin sections in plane- and cross-polarized light were used for verification purposes throughout the process.

The following was carried out for each of the six mineral classes in each of the thin sections: A predetermined number of crystals (25, 50 or 100) was randomly selected in Adobe Photoshop. Random selection consists of assigning a uniform probability distribution to all points falling within the limits of the digitized specimen (rectangular thin section). A crystal is selected if the pair of random coordinates (generated from a uniform distribution) falls within its limits, and the crystal falls entirely within the bounds of the specimen. Crystals larger than 25 μm could be reliably identified. By using the ‘quick selection tool’ in Photoshop the crystals were converted to paths in vector format and given a corresponding mineral-class colour. All in all, about 14,000 crystals were digitized. The images were exported and loaded into the JMicrovision software for segmentation and data acquisition of 16 features including length, width, area, perimeter, and equivalent

circular diameter. The equivalent circular diameter (D_2) was chosen as the feature for further data analysis, in accordance with the assumption that crystals are spherical. The distributions of equivalent circular diameter (D_2) were subsequently converted to 3-D and fused with the 1-D intercept data of Heins (1992) under the assumption of a lognormal frequency distribution of crystal size. The lower limit on crystal size in the data of Heins (1992) is 10 µm. The upper limit on crystal size is given by the smallest dimension of the rectangular specimens, i.e., ~25 mm. The stereological method used to estimate the crystal-size distributions is discussed in detail in [Appendix A](#).

Unfortunately, the data set of the sediments does not include measurements of property 3, so we cannot compare directly CSPDs of parent rocks and sediments. We will, therefore, limit ourselves to presenting the two parameters of the best-fit lognormal distributions (mean and standard deviation) of each mineral in each of the thin sections of the parent rocks separately, as well as the average values for the minerals in each pluton. All distributions will be compared against the observations by means of four statistical goodness-of-fit tests: Anderson-Darling, Pearson's Chi-squared, Kolmogorov-Smirnov, and Shapiro-Wilk (e.g., [Stephens, 1974](#); [Davis, 2002](#) and references therein).

4.3. Representation of fundamental properties

The first two fundamental properties of rocks (modal and interface data) represent compositional quantities and are thus preferentially analysed in the form of log-ratios ([Aitchison, 1982, 1986](#); [Pawlowsky-Glahn et al., 2015](#)). We will use the centred log-ratio (clr) transformation. The clr-vector corresponding to an arbitrary vector \mathbf{z} with k components $\mathbf{z} = [z_1, \dots, z_j, \dots, z_k]$ is defined as:

$$\mathbf{y} = \text{clr}(\mathbf{z}) = [\ln(z_1) - h(\mathbf{z}), \dots, \ln(z_j) - h(\mathbf{z}), \dots, \ln(z_k) - h(\mathbf{z})],$$

$$h(\mathbf{z}) = \frac{1}{k} \sum_{j=1}^k \ln(z_j)$$

All statistical calculations will be performed in clr-space. If required, the inverse clr-transform may be applied to express fundamental properties in terms of their native units. The inverse clr-transformation is defined as:

$$\mathbf{z} = \text{clr}^{-1}(\mathbf{y}) = \psi^{-1}[\exp(y_1), \dots, \exp(y_j), \dots, \exp(y_k)], \quad \psi = \sum_{j=1}^k \exp(y_j)$$

Because clr-transformed data can be treated with standard statistical methods ([Pawlowsky-Glahn et al., 2015](#); [van den Boogaart and Tolosana-Delgado, 2013](#)), we start by examining if differences among the properties of parent rocks and their derived sediments are considered statistically significant at a 0.05 level. This involves the calculation of the vector means and variance-covariance matrices of each subset of samples (representing the parent (P), and the coarse (C), medium (M), and fine (F) sand fractions) belonging to a single pluton. Under the assumption that the data follow a multivariate normal distribution, we applied the two-sample version of Hotelling's T^2 test to each pair of subsets (e.g., [Davis, 2002](#), p. 479–483).

Multivariate analysis of properties 1 and 2 was carried out employing Principal Components Analysis (PCA). The results were graphically summarized in biplots which show the data points in a space of reduced dimensionality, as determined by the singular value decomposition of the data matrix ([Aitchison and Greenacre, 2002](#); [van den Boogaart and Tolosana-Delgado, 2013](#)). Dimension reduction through PCA brings out the maximum variability, which implies that the pattern displayed by the data points in the first two dimensions (principal components) may already capture much of the total variability. The measure of total variability captured in each biplot is given by the cumulative proportion of the variance (CPV). A biplot of a series of clr-vectors permits simultaneous evaluation of the specimens (data points)

and loadings (the components of the property vector) in a single graph. If the principal components are represented as unit vectors, the Euclidian distances between data points are a direct measure of compositional dissimilarity in the space of reduced dimensionality.

4.4. SGE trajectories of properties 1 and 2

Our exploratory data analysis of properties 1 and 2 is based on the following line of reasoning, illustrated for the interface composition (property 2). The probability of survival of interfaces mirrors their relative strengths under the prevailing conditions. The interface composition of the rock-fragment assemblage evolves from that of its parent by preferential destruction of the weakest interfaces, which causes enrichment of the strongest interfaces ([Heins, 1992](#)). If breakage of a large rock fragment along relatively weak interfaces produces one or multiple smaller rock fragments, the latter will become even more enriched in relatively strong interfaces. Rock fragments generated from crystalline parent rocks are therefore expected to display a compositional trend of increasing interface strength with decreasing grain size. This effect will be even more prominent because the strength of any given type of crystal interface is expected to be inversely proportional to its area ([Erkan, 1970](#); [Simmons and Richter, 1976](#)). Therefore, SGE trajectories of property 2 in the form of PCMF (Parent, Coarse, Medium, Fine) trends that track the evolution from parent to fine sand should be broadly consistent with an increase of average interface stability. The CSPDs of minerals in rock fragments (property 3) are expected to be biased towards smaller crystal sizes relative to the CSPDs of their parents, because (1) the average crystal size in granitoids is close to that of the sand fraction, and (2) large crystals split off easily owing to their larger (weaker) interface areas and are more likely to be observed as individual grains.

The relative abundances of the different types of crystal interfaces in the parent rock define the initial conditions for sediment generation ([Heins, 1995](#); [Caracciolo et al., 2012](#); [Weltje et al., 2018](#)). If classes of mineral interfaces possess characteristic relative strengths, the evolution of the composition of rock-fragment assemblages shed by different parent rocks should follow parallel SGE trajectories in centred log-ratio space, and the spread among these trajectories should reflect differences among initial conditions (i.e., parent-rock texture and composition), which define the starting point of each trajectory. Hence, if the effects of variable parent-rock texture and composition can be eliminated from interface data, relative interface strengths could be reliably estimated if all trajectories collapse into a single one ([Weltje et al., 2018](#)). The evolution of the modal (mineral) composition of parent rocks and derived sediments can be modelled in the same way.

In the multivariate analyses that follow, we will normalize the data corresponding to each pluton by the mean composition of the parent to eliminate the effects of parent-rock properties on the properties of the derived sediments, i.e., we will only look at changes relative to the parent. If the mean value of the property of interest in the parent rock is given by $\bar{\mathbf{z}}_P$ and the same property in the derived sediment is given by \mathbf{z}_S , (where $S \in \{C, M, F\}$), the change from the parent to the sediment is represented by an additive operation in the clr-space (i.e., a shift):

$$\mathbf{S}^* = \text{clr}(\Delta\mathbf{z}_{PS}) = \text{clr}(\mathbf{z}_S) - \text{clr}(\bar{\mathbf{z}}_P), \text{ where } \mathbf{S}^* \in \{C^*, M^*, F^*\}.$$

In this framework, the data points \mathbf{S}^* represent the compositional change of sediment fraction S relative to the mean composition of its parent, i.e., an SGE trajectory. This data transformation is essential for examining if compositional trends can be described with a single model because the degree to which trends diverge tells us something about the predictability of the direction in which modal or interface compositions evolve during sediment generation. We will present a series of such analyses of the SGE trajectories of properties 1 and 2 in an attempt to extract common patterns from the six plutons analysed previously by [Heins \(1992\)](#).

The shift introduced above to eliminate the variability of “inherited” properties from the data set is identical to the transformation that was

used to define the interface composition (property 2) as a fundamental property which is independent of the modal composition because it is expressed relative to the expected interface composition under the assumption of random texture $\text{clr}\{\alpha\} = \text{clr}(f) - \text{clr}(f^*)$.

Note that random texture of rock-fragment assemblages implies that all interfaces are equally stable, a hypothesis that can be evaluated with a Chi-squared test, as illustrated in Weltje et al. (2018).

4.5. Weighted mean SGE trajectories

The last phase of exploratory data analysis consists of subjecting the mean compositions of the parents and the sediment fractions (properties 1 and 2) to a weighted PCA. For each pluton, the mean composition of the parent rock was subtracted from the mean composition of each sediment fraction to define mean SGE trajectories, as described in the previous section. The “weight of evidence” assigned to each of these mean SGE trajectories was derived using the rules of error propagation:

$$w_{PS} = \left(\frac{\text{Tvar}(P)}{n_p} + \frac{\text{Tvar}(S)}{n_s} \right)^{-0.5}.$$

Where Tvar represents the total variance of the property in the parent (P) and the derived sediment (S). The total variance is given by the sum of the variances of the elements in the sample, and n stands for the sizes of the sample from which this mean property has been estimated (Table 1). Each vector of compositional change was weighted (multiplied) by w_{PS} , and then the complete data set of all six plutons was subjected to PCA. The results of the weighted PCA were used to derive a reduced-rank estimate of the mean SGE trajectories by selecting the number of dimensions for which around 95% of the variability could be described, assuming that there is at least 5% noise in the data. The reduced-rank estimates were subsequently rescaled by dividing each vector by w_{PS} to give reweighted “filtered” estimates of the mean SGE trajectories. The final results of our statistical analysis are summarized in a series of biplots which were constructed by subjecting the reweighted “filtered” SGE trajectories to a conventional PCA. This last step permits straightforward visualisation and interpretation of the patterns in terms of the elements of compositional change (the loadings of the elements on the principal components). The amount of information retained in this way may be visualized with dimension-variance plots.

5. Results

5.1. Mineral composition (properties 1a and 1b)

This property is represented by the bulk mineral composition of the sediments relative to the composition of their parents (property 1a). A separate analysis was conducted of the mineral composition of the rock-fragment assemblages in the sediments relative to the composition of their parents (property 1b). Five classes of elements were considered: quartz (Q), plagioclase (P), K-feldspar (K), biotite (B), and an others (Oth.) group comprising opaque minerals (O) and translucent accessory minerals (A) of which the most abundant are hornblende and chlorite. Hence, $m = 5$.

The results of Hotelling's two-sample T^2 tests (Table 2) show that in terms of the bulk mineral composition (property 1a), there is hardly any differentiation among P (Parent) and C (Coarse) or M (Medium) and F (Fine). Significant differences are only observed in pluton GR for PC and MF and in pluton CA-NS for MF . Differences between P and M , and/or P and F , on the other hand, are significant for most plutons (11 out of 12). There is notable differentiation among the C , M , and F fractions (12 out of 18). Pluton AZ (which is the finest-grained pluton, see Table 1) shows no differentiation among the three sediment fractions (CM , CF and MF in Table 2). Overall, 24 out of 36 differences are significant. In terms of the mineral compositions of the parent rocks relative to those

Table 2

Results of Hotelling's two-sample T^2 tests. Differences among means of P , C , M , and F are either significant (+) or not significant (−) at a level of 0.05. ¹ bulk modal composition; ² modal composition of rock-fragment assemblage; ³ interface composition.

Property 1a ¹	PC	PM	PF	CM	CF	MF
AZ	−	+	+	+	+	−
CA-EW	−	+	+	+	+	−
CA-NS	−	+	+	+	+	+
GR	+	+	+	−	+	+
MT	−	+	+	+	+	−
WA	−	−	+	−	+	−
Property 1b ²	PC	PM	PF	CM	CF	MF
AZ	−	+	+	+	+	−
CA-EW	−	+	+	+	+	−
CA-NS	+	+	+	+	+	−
GR	+	+	+	−	+	−
MT	−	+	+	+	+	−
WA	−	−	+	+	+	−
Property 2 ³	PC	PM	PF	CM	CF	MF
AZ	−	+	+	−	+	+
CA-EW	+	+	+	+	+	+
CA-NS	−	+	+	+	−	−
GR	−	+	+	+	−	−
MT	+	+	+	+	+	+
WA	−	−	−	−	−	−

of the rock-fragment assemblages (property 1b), results are broadly similar, albeit slightly more conspicuous. All differences between P and F , and C and F are significant. Overall, 24 out of 36 differences are significant.

The biplots of properties 1a (Fig. 2) and 1b (Fig. 3) display broadly similar patterns. The amount of information retained in both plots is large: the cumulative proportion of variance (CPV) equals 91% in the former and 89% in the latter. The mean composition of the parents (P) appears at exactly the same location in each set of biplots owing to the fact that the properties of the sediments of each pluton have been normalized relative to the mean property of their parents. Systematic variations of the bulk mineral composition relative to the inherited modal composition of parents show comparable patterns among plutons (Fig. 2), which indicates that compositional shifts are fairly predictable. The average PCM trend in the biplots of Fig. 2 is from right to left, which implies a relative decrease of Q and K, and a relative increase of P and Oth. and/or B. Systematic variations of the mineral composition of the rock-fragment assemblages relative to the inherited modal composition of their parents also show comparable patterns among plutons (Fig. 3), which indicates that compositional shifts within the rock-fragment assemblage are also fairly predictable. The most common PCM trend in the biplots of Fig. 3 is from left to right, which implies a relative decrease of Q and K, and a relative increase of B and Oth.

5.2. Interface composition (property 2)

This property has been quantified in terms of isostructural interfaces (all combinations among Q, P, and K, 6 in total) and a rest or remaining group comprising the sum of all non-isostructural interfaces (all interfaces involving B and A, 9 in total). Opaque minerals (O) were left out of the interface data, as OO interfaces cannot be reliably measured in transmitted light. Summation of non-isostructural interfaces was motivated by the results of previous studies (Heins, 1995; Caracciolo et al., 2012), which showed that non-isostructural interfaces are expected to be weakest. Hence, $k = 7$.

The results of Hotelling's two-sample T^2 tests (Table 2) show that there is usually no difference between P and C , nor between M and F . One pluton (WA) does not show any significant difference among P , C , M , and F . The degree of contrast among interface compositions seems to be less than that of properties 1a and 1b. Overall, 22 out of 36 pairs

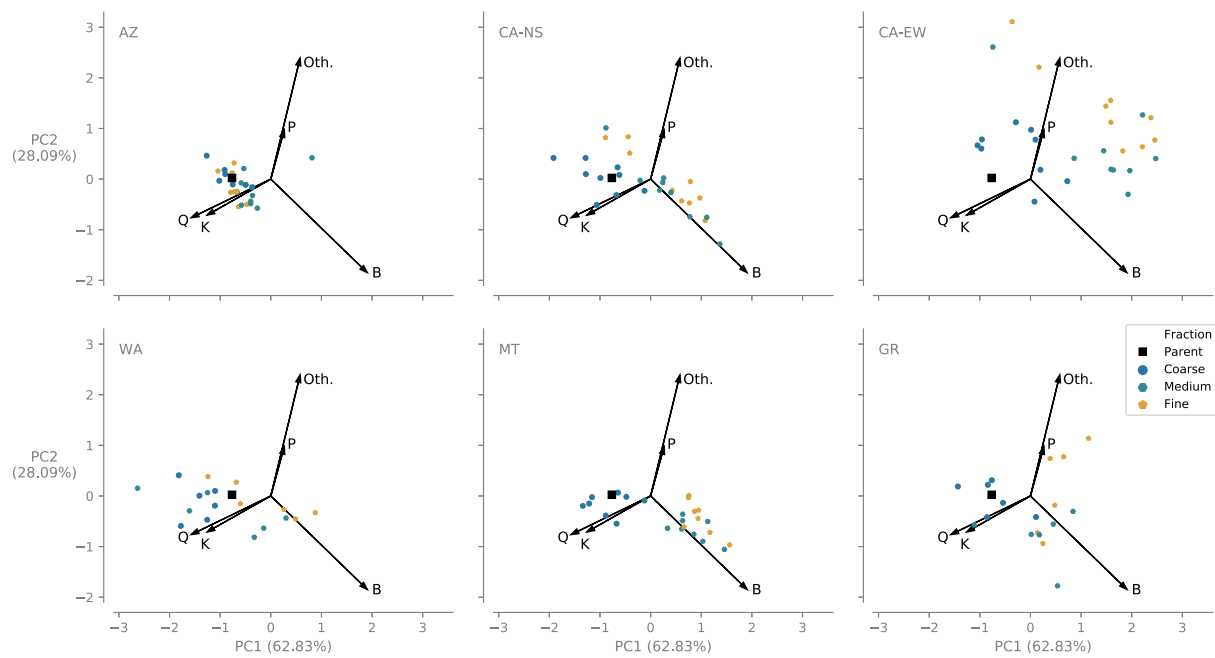


Fig. 2. Biplots of bulk modal composition (Property 1a) of coarse-medium-fine sand fractions corrected for the average composition of their parents (separately for each pluton). CPV = 91%.

show significant differences.

The biplots of property 2 (Fig. 4) illustrate the systematic deviations of interface frequency distributions among parents and derived sediments. The directions and magnitudes of deviations from the inherited interface frequency distribution of parents vary strongly among plutons, which is also brought out by the fact that CPV = 63% only, and up to 4 dimensions may be needed to fully capture the signal of this property. It appears that relative stability of interfaces varies systematically within each pluton, but differences among plutons are significant and a general PCMF trend cannot be identified.

5.3. Crystal-size probability distributions (property 3)

The CSPDs of the minerals in each of the parent rocks have been estimated by assuming that they follow a lognormal frequency distribution (for details see Appendix A). The results of the stereological inversion were evaluated through four goodness-of-fit tests on the

modelled CSPDs at a significance level of 0.05: Anderson-Darling (AD), Kolmogorov-Smirnov (KS), Pearson's Chi-squared (PC), and Shapiro-Wilk (SW) (e.g., Stephens, 1974; Davis, 2002 and references therein). The tests were run on CSPDs determined from individual thin sections, as well as on bulk CSPDs estimated from pooling all observations from a single pluton pertaining to a single mineral class. The results of the tests are summarized in Table 3 (test results of the individual thin sections are included in the online supplementary material).

The most conspicuous result is the strong positive correlation among the AD, PC, and SW tests, which implies a high degree of consistency. Table 3 also indicates that the KS test is much too forgiving, as already noted by Higgins (2006b). We will, therefore, base our conclusions solely on the three former tests. Approximately 87% of the CSPDs measured in individual thin sections pass the lognormality tests, whereas only 62% of the CSPDs fitted to the pooled data of each pluton pass the test.

A lognormal distribution of D implies a normal distribution of $\ln(D)$.

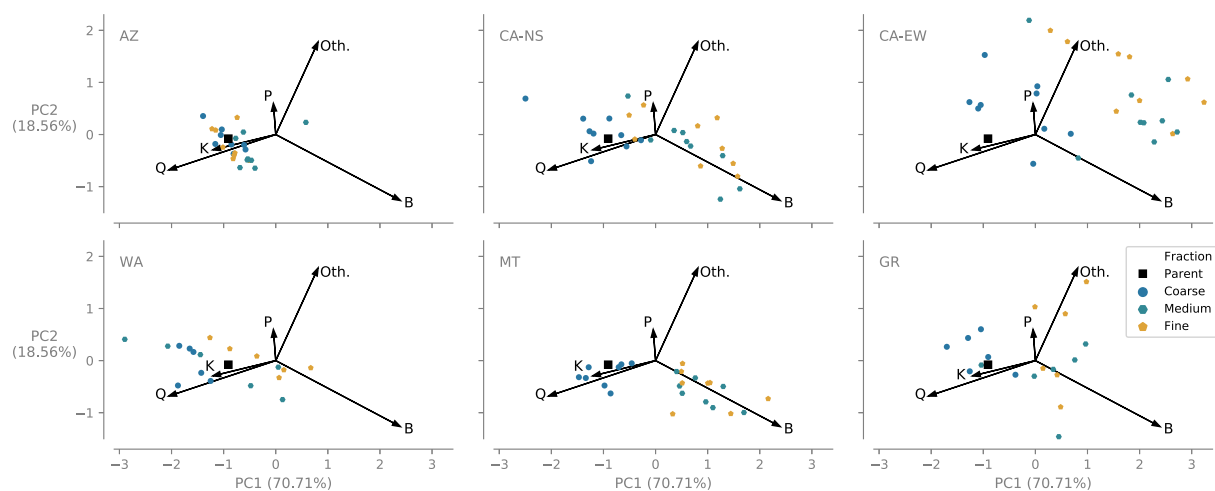


Fig. 3. Biplots of the modal composition of rock-fragment assemblages (Property 1b) in coarse-medium-fine sand fractions corrected for the average composition of their parents (separately for each pluton). CPV = 89%.

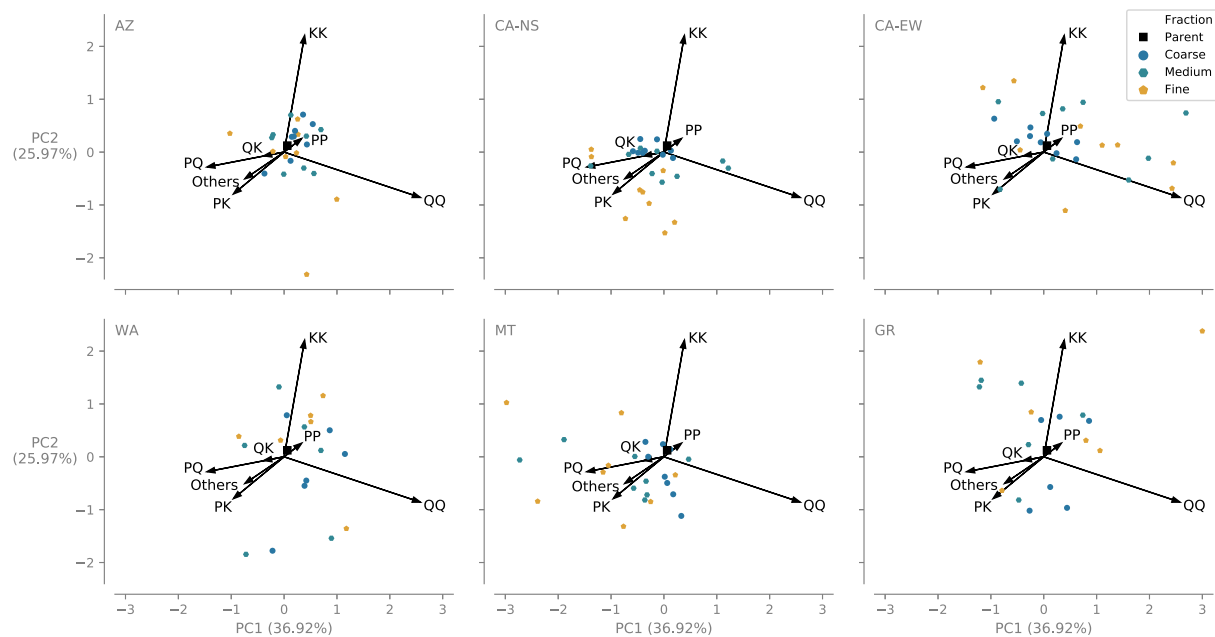


Fig. 4. Biplots of interface composition of coarse-medium-fine sand fractions (Property 2) corrected for the average composition of their parents (separately for each pluton). CPV = 63%.

Table 3

Summary of statistical tests of CSPDs on the level of plutons (*p*-values reported) and individual specimens (reported as the number of specimens out of the total (*n*) that pass the test). AD = Anderson-Darling test, PC = Pearson's Chi-squared test, KS = Kolmogorov-Smirnov test, SW = Shapiro-Wilk test. A significance level of 0.05 was used throughout.

Pluton	Mineral	<i>n</i>	AD		PC		KS		SW	
			Plutons	Samples	Plutons	Samples	Plutons	Samples	Plutons	Samples
AZ	Q	15	FAIL	9	0.000	10	0.356	14	0.000	9
	P	15	FAIL	11	0.013	15	0.144	15	0.000	12
	K	15	FAIL	12	0.000	13	0.048	15	0.000	13
	B	15	PASS	13	0.340	13	0.667	15	0.125	10
	O	15	FAIL	15	0.324	15	0.128	15	0.040	13
	A	15	FAIL	14	0.152	12	0.059	15	0.000	13
CA-EW	Q	6	FAIL	3	0.013	6	0.127	6	0.002	3
	P	6	PASS	6	0.895	6	0.945	6	0.480	6
	K	6	PASS	5	0.434	5	0.432	6	0.020	5
	B	6	FAIL	3	0.059	5	0.240	6	0.000	3
	O	6	PASS	6	0.771	6	0.871	6	0.921	6
	A	6	PASS	4	0.062	5	0.799	6	0.536	4
CA-NS	Q	5	PASS	4	0.041	4	0.309	5	0.142	4
	P	5	PASS	5	0.604	5	0.989	5	0.257	5
	K	5	FAIL	4	0.104	5	0.144	5	0.006	4
	B	4	FAIL	2	0.036	4	0.104	4	0.001	3
	O	5	PASS	5	0.666	5	0.789	5	0.114	4
	A	5	PASS	5	0.527	5	0.994	5	0.942	5
GR	Q	10	FAIL	6	0.002	8	0.490	10	0.001	5
	P	10	PASS	8	0.528	9	0.644	10	0.017	8
	K	10	FAIL	9	0.000	7	0.266	10	0.000	8
	B	10	FAIL	10	0.157	10	0.625	10	0.000	10
	O	9	PASS	9	0.385	9	0.651	9	0.243	9
	A	10	PASS	10	0.506	10	0.887	10	0.524	10
MT	Q	8	PASS	5	0.927	6	0.768	8	0.155	6
	P	8	FAIL	7	0.011	7	0.151	8	0.020	7
	K	8	FAIL	8	0.211	8	0.524	8	0.002	8
	B	8	PASS	7	0.979	8	0.907	8	0.004	7
	O	8	FAIL	8	0.008	7	0.186	8	0.158	8
	A	8	PASS	8	0.563	8	0.929	8	0.808	8
WA	Q	4	PASS	4	0.783	4	0.871	4	0.513	4
	P	4	PASS	4	0.077	4	0.502	4	0.292	4
	K	3	PASS	3	0.570	3	0.873	3	0.290	3
	B	4	PASS	2	0.960	4	0.989	4	0.840	4
	O	0	na							
	A	4	PASS	4	0.494	3	0.848	4	0.497	4

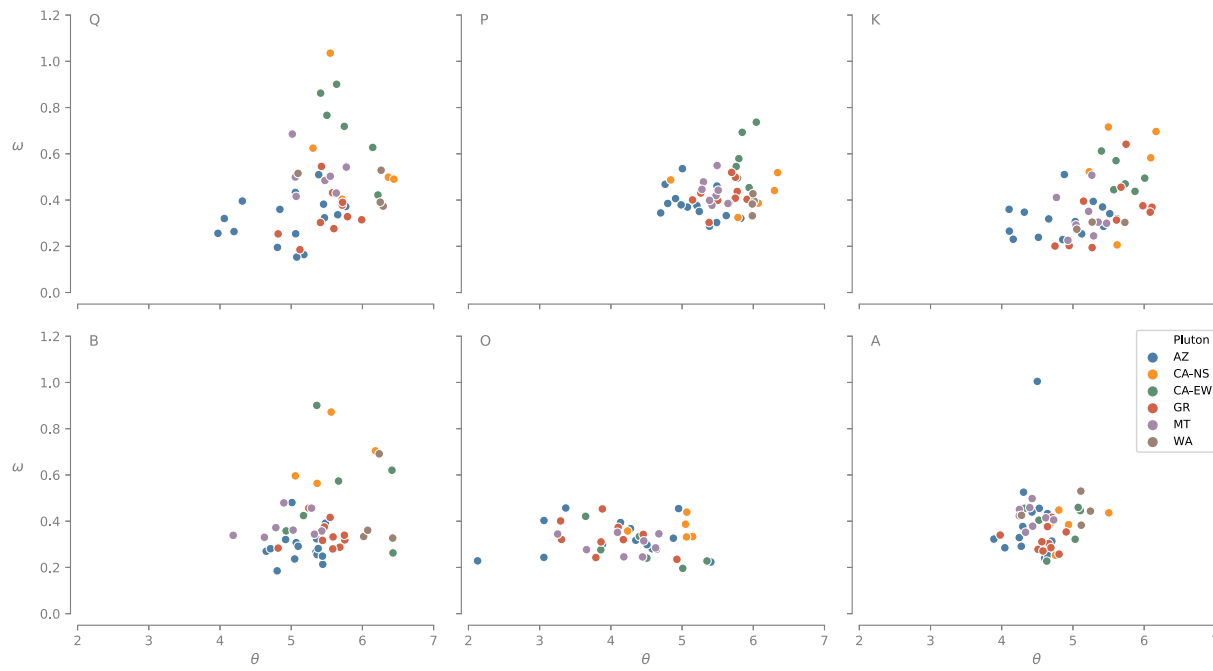


Fig. 5. Crystal-size distributions of QKPBOA estimated from individual specimens: mean versus standard deviation of normal distributions of $\ln(D)$.

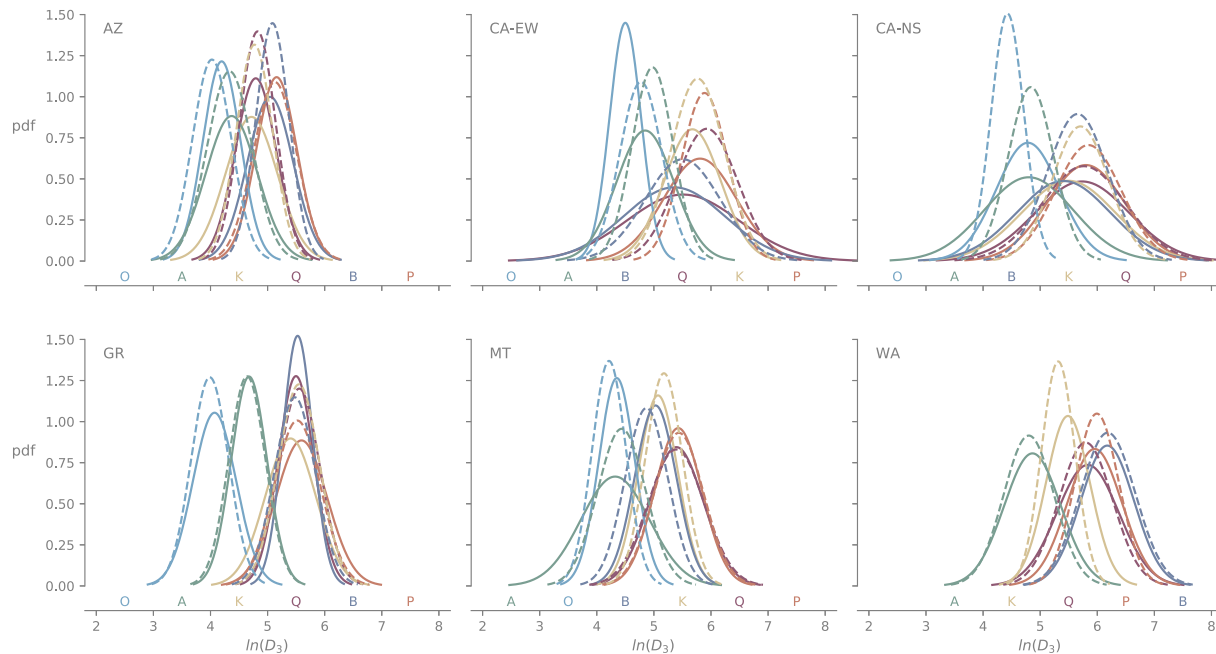


Fig. 6. Lognormal CSPDs of each pluton, shown as normal distributions of $\ln(D)$ estimated from the pooled data of each pluton (solid lines). The average CSPDs of each pluton (dashed lines) are shown for comparison. The difference between the two reflects the degree of spatial heterogeneity (Table 5).

The means and standard deviations of the normal distributions of $\ln(D)$ as determined from individual thin sections are displayed in Fig. 5. For each mineral, the variability of model parameters within a single pluton is smaller than the variability among plutons. This is brought out by the degree of clustering of model parameters in Fig. 5. Uncommon exceptions to this clustering may be present as is the case for mineral class A in sample AZ-89-008 which displays hornblendes up to 0.7 cm in length. The clustering provided the justification for estimating a single CSPD of each mineral within a pluton. Fig. 6 shows the distributions determined by pooling all data pertaining to a given mineral class for each pluton (i.e., the average crystal-size distributions per pluton as given in Table 4). The order of mean crystal size (from smallest to

largest) is OA(B, K, Q)P except for pluton WA which shows AKQP (O was not measured because it was not commonly present). The order of (B, Q, K) differs between the remaining five plutons and is BKQ in plutons CA-NS and MT, KQB in plutons AZ and GR, whereas only one pluton (CA-EW) shows the order BQK (Table 4).

Upscaling to the lithosome level is exemplified by fitting a single distribution to all crystals of a given mineral counted in the set of specimens (thin sections) belonging to a single pluton. For each pluton, the lognormal CSPD obtained from the pooled data was compared to the average of the CSPDs of the corresponding mineral as determined from individual thin sections (i.e., the models obtained by pooling the CSPDs) with a PC test. A visual comparison of both versions of the

Table 4

Estimated parameters of the lognormal distribution of crystal size. D [μm] is the geometric mean crystal diameter. M and S are the mean and standard deviation of the normal distribution of $\ln(D)$, respectively.

Pluton	Mineral	D [μm]	M ($\ln D$)	S ($\ln D$)	# crystals
AZ	Q	121	4.793	0.359	1500
	P	174	5.158	0.356	750
	K	112	4.717	0.455	750
	B	155	5.046	0.399	750
	O	66	4.195	0.328	750
	A	79	4.370	0.452	750
CA-EW	Q	247	5.509	0.986	300
	P	333	5.808	0.640	150
	K	292	5.675	0.497	150
	B	212	5.356	0.889	150
	O	90	4.499	0.275	150
	A	127	4.848	0.502	150
CA-NS	Q	309	5.734	0.823	250
	P	330	5.800	0.683	125
	K	244	5.495	0.817	125
	B	223	5.407	0.819	100
	O	120	4.785	0.554	125
	A	122	4.800	0.782	125
GR	Q	244	5.497	0.312	1000
	P	269	5.593	0.450	500
	K	222	5.402	0.444	500
	B	251	5.526	0.262	500
	O	59	4.071	0.378	500
	A	107	4.676	0.313	500
MT	Q	220	5.395	0.472	800
	P	227	5.427	0.415	400
	K	160	5.072	0.344	400
	B	153	5.029	0.363	400
	O	78	4.351	0.315	400
	A	75	4.321	0.599	400
WA	Q	342	5.835	0.542	200
	P	385	5.954	0.478	100
	K	241	5.486	0.386	75
	B	481	6.176	0.467	100
	O	-	-	-	0
	A	130	4.865	0.494	100
Total					14,025

Table 5

Results (p-values) of the Chi-squared test of the two CSPDs obtained by (1) pooling the data and (2) pooling the CSPDs at a significance level of 0.05.

	Q	P	K	B	O	A
AZ	0.435	1.000	0.000	0.000	1.000	0.010
CA-EW	0.000	0.993	1.000	0.000	1.000	0.581
CA-NS	0.000	0.000	0.000	0.309	0.002	0.000
GR	1.000	1.000	0.000	0.995	0.996	1.000
MT	1.000	1.000	1.000	1.000	1.000	0.000
WA	0.814	0.839	0.830	0.959	na	0.994

pooling is presented in Fig. 6. In this illustration, the models resulting from the calculated distribution parameters are displayed rather than the raw data that were used in the PC test. The magnitude of the discrepancy between the two distributions serves as a guide to the magnitude of spatial variability of a lithosome. The results of the PC test are summarized in Table 5. Row-wise inspection of Table 5 shows that three plutons (GR, MT, WA) appear to be fairly homogeneous because the CSPDs of 5 out of 6 minerals pass the test. The other three plutons (AZ, CA-EW, CA-NS) display (much) stronger spatial variability of CSPDs, in particular CA-NS. Column-wise evaluation shows that mineral classes P, B, Q and O tend to display the lowest degree of spatial variability, whereas the CSPDs of K and A tend to be more variable and cannot be approximated by lognormal distributions at the level of a lithosome.

5.4. Weighted mean SGE trajectories

The biplots of Fig. 7 bring out the main features of SGE trajectories of properties 1a, 1b, and 2. The overall PCMF trends of modal composition (properties 1a and 1b) are almost identical. They indicate that relative to the parent, the overall compositional trend from coarse to fine sand is characterized by a relative decrease of Q and K, a relative increase of B, and variable behaviour of P and Oth. (the rest group comprising O and A). Even plutons CA-NS and MT, which display the most divergent PCMF trends, seem to have comparable CMF trajectories, characterized by: B > Oth. > P > K > Q. This trajectory indicates that with decreasing grain size, both the bulk sediment and the rock fragments tend to become enriched in B and Oth., and depleted in Q and K.

The PCMF trends of interface compositions (property 2) are more diverse. Apart from a general evolution towards decreasing QK and PP interfaces, and increasing QQ and PK interfaces (bottom to top in the biplot), there is quite a bit of variation among PQ, KK, and the Others group comprising all non-isostructural interfaces. In plutons AZ and GR, which seem to follow the average trend, there is hardly any change among these three groups. Interfaces in these two plutons arranged in order of decreasing stability form the following series: QQ > PK > (QP ≈ KK ≈ Others) > PP > QK. Plutons CA-EW and MT display the following pattern in order of decreasing stability: (PK ≈ Others ≈ QP) > (QK ≈ QQ) > (KK ≈ PP). For plutons CA-NS and WA, the corresponding pattern is: QQ > KK > PP > (PK ≈ Others ≈ QP) > QK. Plutons MT and WA seem to represent the end-member cases. As seen in the biplot of Fig. 7, the evolution of these two plutons is diametrically opposite. However, PCMF trends for individual plutons and their derived sediments are persistent and clear.

Fig. 8 clarifies the amount of information retained in the filtering process. The PCMF trends of property 1 preserve almost 100% of the filtered data, equal to ~95% of the variance of the unfiltered data (Fig. 8a, b), whereas those of property 2 (Fig. 8c) cannot be properly visualized in 2-D. Up to four dimensions would be needed to fully capture the variability among the PCMF trends of interface evolution displayed by the six plutons analysed in this study.

6. Discussion and conclusions

6.1. The Generalized Griffiths Descriptor

The GGD proposed in this study permits a wide range of rocks and their derived sediments to be described in terms of the same fundamental properties, which opens the way to statistically rigorous analysis of SGE trajectories, testing of petrogenetic hypotheses, and simulation of rocks possessing arbitrary combinations of fundamental properties. It should be borne in mind that highly condensed statistical representations of complex 3-D aggregates as presented in this contribution are unlikely to cover all possible cases. For instance, the GGD cannot be used to describe biogenic carbonates (boundstones). The GGD as implemented in this study was designed with the objective to describe a wide variety of igneous, metamorphic, and siliciclastic parent rocks and their detritus at the thin-section scale, subject to achieving a balance between simplicity and generic applicability. In our attempt to define the GGD for granitoids and their sand-sized detritus as a tool for siliciclastic SGE studies, one major simplification had to be made. All elements of the rock were assumed spherical, so as to eliminate properties 4 and 5 from the current implementation of the GGD. If desirable and feasible, properties 4 and 5 of the GGD may be activated using appropriate statistical descriptions of shape and orientation data.

6.2. Digital image analysis

In principle, estimates of all fundamental properties of a specimen

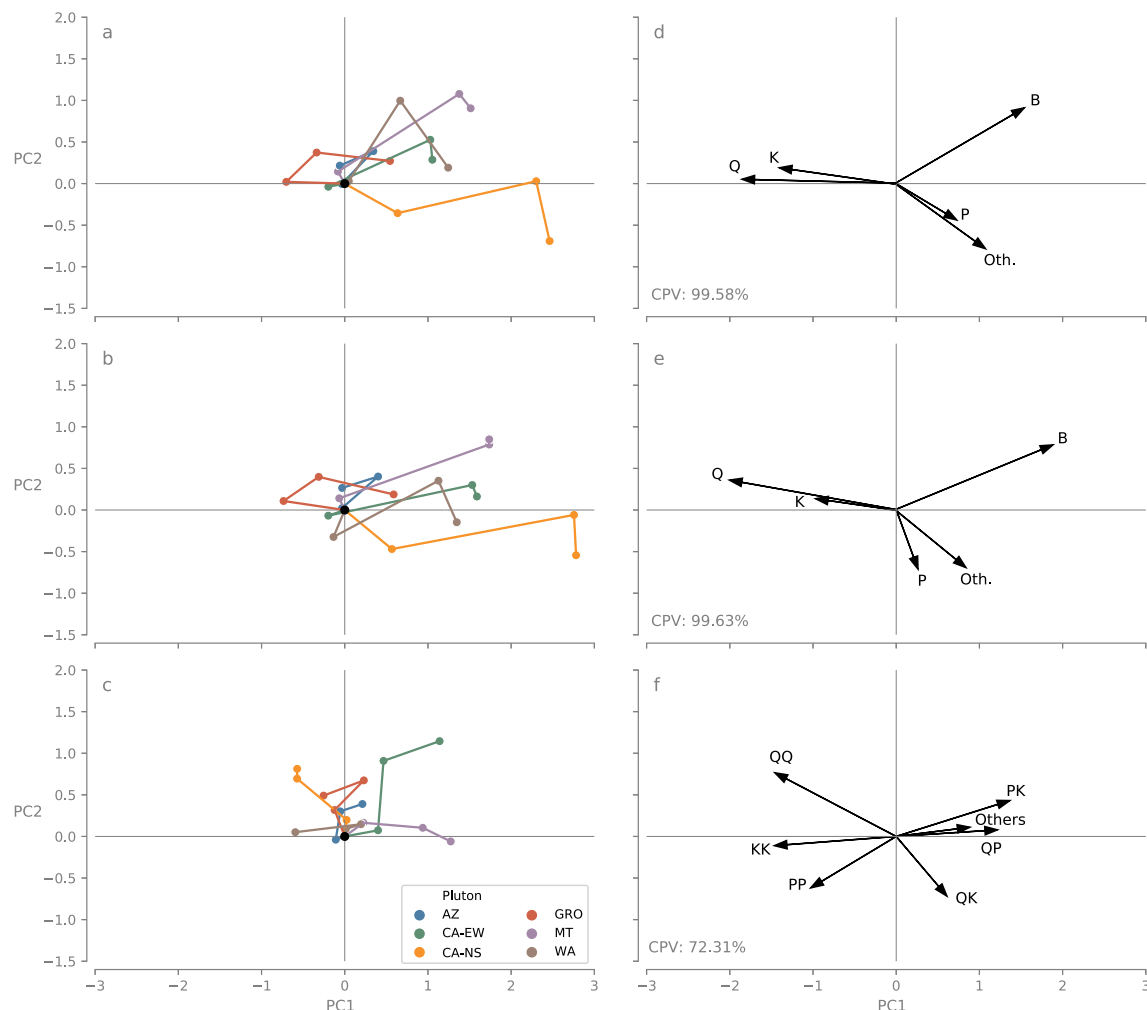


Fig. 7. Biplots of weighted “filtered” mean SGE trajectories of properties 1a (a & d), 1b (b & e), and 2 (c & f). Because P is located at the origin (black dot), the three data points show the composition of coarse-medium-fine sand fractions corrected for the average composition of their parents. PCA scores are plotted on the first column and PCA loadings on the second column.

can be obtained through digital image analysis of thin sections which have been segmented into petrographic classes (Armienti and Tarquini, 2002; Tarquini and Favalli, 2010; Caracciolo et al., 2012). The 2-D modal composition (property 1) and the 1-D interface composition (property 2) acquired in thin section are equivalent to their 3-D counterparts. A generic data-acquisition protocol should be designed to capture the 3-D properties of rocks that may not be considered isotropic at the thin-section scale. It is recommended to analyse three orthogonal cuts through each specimen to capture the main direction(s) of anisotropy. The size (property 3), shape (property 4), and orientation

distributions (property 5) of the phases measured in sets of orthogonal thin section must be simultaneously converted from 2-D to 3-D by means of stereological methods (cf. Cruz Orive, 1976, 1978).

6.3. Crystal-size probability distributions

The degree of clustering of CSPD parameters in Fig. 5 indicates that characteristic CSPDs can be established for each pluton. In absence of evidence to the contrary, the characteristic CSPDs have been modelled as lognormal size-frequency distributions. Many more crystals would

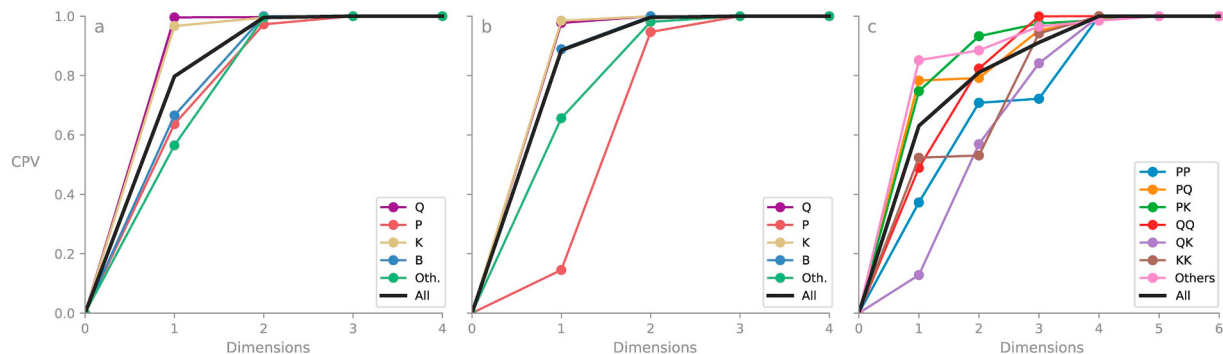


Fig. 8. Plots showing CPV as a function of the number of dimensions for the weighted “filtered” mean SGE trajectories in Fig. 7.

have to be measured to establish whether or not this assumption holds because the fitting of suitable models to CS(P)D data requires that the tails of the distributions have been adequately sampled (Higgins, 2000, 2006b). Given the current state of SGE modelling, establishing accurate CSPD models is not considered to be a matter of the highest priority. Our objective is to establish a baseline estimate of the mode of occurrence of the most abundant mineral phases in parent rocks on the scale of entire drainage basins. Based on our test results, and in view of the uncertainties surrounding the estimation of 3-D size distributions from finite 2-D samples, we conclude that the lognormal distribution is an acceptable default CSPD model for SGE studies of granitoids.

6.4. Stability of minerals

Systematic variations of the bulk mineral composition relative to the inherited modal composition of parents show comparable patterns among plutons, which indicates that compositional shifts are fairly predictable. The same applies to the mineral composition of the rock-fragment assemblages. The most common PCMF trend in the biplots of Fig. 7 is from left to right, which implies a relative decrease of Q and K, and a relative increase of B and Oth. (the group comprising O and A).

Even plutons CA-NS and MT, which display the most divergent PCMF trends, seem to have comparable CMF trajectories, characterized by: B > Oth. > P > K > Q. This trajectory indicates that with decreasing grain size, both the bulk sediment and the rock fragments tend to become enriched in B and Oth., and depleted in Q and K. The simplest possible explanation for the PCMF trends in Fig. 7 is that monocrystalline Q and K grains tend to accumulate in the very fine sand and silt fractions. Selective removal of Q and K from the medium and fine sand fractions would be sufficient to explain the relative increase of B, Oth., and/or P with decreasing grain size.

The conclusions drawn from two detailed studies of weathering products of granitoid parent rocks produced under conditions in which either mechanical or chemical weathering are considered the dominant control on sediment generation (von Eynatten et al., 2012, 2016) confirm the spectrum of (P)CMF trends observed in this study. In the case of the Sila Massif (Italy), where sediment generation is strongly influenced by chemical weathering, the mineralogy behind the geochemical data reflects an overall decrease of quartz and K-feldspar over the full grain-size range from coarse to fine. This is compensated by an overall increase of sheet silicates from coarse to fine, where the increase of clay minerals strongly outpaces the increase of micas in the silt to clay fractions (von Eynatten et al., 2016). The compositional data of the Aar Massif (Switzerland), which represent a case of pure mechanical weathering, show a linear trend describing preferential enrichment of phyllosilicates at the expense of quartz and feldspar towards finer fractions, with breaks at certain grain-size thresholds. The observed pattern describes the process of comminution: the most durable minerals such as quartz are concentrated close to their inherited grain-sizes whereas less durable minerals are enriched in silt fractions, and the least durable minerals (i.e., sheet silicates) are enriched in the very fine silt to clay fractions (von Eynatten et al., 2012). Peaking of quartz and total SiO₂ concentrations in fine to very fine sand may be ascribed to mechanical comminution, mineral durability, and inherited grain-size distribution in the glacial Aar case study (von Eynatten et al., 2012). This is not observed in the chemically weathered sediments of the Sila Massif (von Eynatten et al., 2016), where instead, both quartz and total SiO₂ concentrations continuously decrease from coarse to fine, reflecting the cumulative effects of minor mechanical forces, quartz leaching, and hydrolysis.

The main compositional trend identified among the six plutons analysed is the overall change in mineral composition with decreasing grain size, attributed to the selective removal of Q and K from the medium and fine sand fractions, and their accumulation in the form of monocrystalline grains in the very fine sand and silt fractions. Quantitative XRD measurements of the very fine sand and silt fractions

would be needed to check this hypothesis and complete the mineral-composition database. Such additional data are also sufficient for establishing the petrographic composition, as polycrystalline grains will be scarce or absent in the size range below fine sand, which implies convergence of mineralogical and petrographic composition.

6.5. Stability of interfaces

During exhumation and weathering, the anisotropy of physical properties of minerals (compressibility and expansibility) creates interface strain owing to unloading, deformation, and temperature variations (Heins, 1995). Interface strengths are expected to differ among isomineralic, isostructural, and non-isostructural interfaces (Heins, 1995). Direct measurement of the tensile strengths of isostructural quartz-feldspar interfaces has shown that they are significantly weaker than the quartz and feldspar grains themselves, although available data suggest that the variability of tensile interface strengths among plutons seems to be in the same range as that within plutons (Savanick and Johnson, 1974). The strength of interfaces is also determined by their morphology because straight crystal interfaces are weaker than more convoluted crystal interfaces that form a tightly interlocked framework (Erkan, 1970). In addition to the above factors which mainly determine the mechanical strength of interfaces, the role of chemical weathering should be taken into consideration because it acts as an important modifier of mechanical interface strength in natural systems (Pye, 1985, 1986).

The analysis of Caracciolo et al. (2012) indicates that under conditions dominated by mechanical weathering, QQ > PP > QP > PK. This result is consistent with the assessment of Heins (1995) regarding the higher preservation potential of isostructural PK and QK interfaces relative to isomineralic KK interfaces. Non-isostructural interfaces, such as those involving B, A, and O are the weakest. If we arrange the interfaces according to Heins (1995) and Caracciolo et al. (2012) in order of decreasing stability, they would form the following series: QQ > PP > QP > (PK ≈ QK) > KK > Others.

None of the three representative series extracted from the results of our interface analysis shows many similarities to this expectation. In addition, the representative series are quite different from each other. From this, we conclude that the evolution of interface composition among plutons cannot be predicted from a general theory about contrasts among isomineralic, isostructural, and non-isostructural interfaces. This observation is consistent with the original premise of Heins (1992) that the relative stability of the interfaces depends on the line of attack (chemical vs. mechanical). The hotter and wetter, the more important is chemical attack. In this respect, it is interesting to note that plutons MT and WA, which seem to represent the end-member cases in terms of relative interface stability, are located in the driest and wettest areas, respectively (Heins, 1992, 1995).

In view of the many factors that are likely to affect the relative strengths of interface classes, it should come as no surprise that the evolution of interface composition as depicted by their PCMF trends turns out to be unique for each pluton. The reason that our general conclusion with respect to relative interface stabilities deviates from those of Heins (1995) and Caracciolo et al. (2012) is that we have defined the interface composition as a fundamental property sensu Griffiths (1961), which implies that it has been decoupled from the modal composition. Heins (1995) and Caracciolo et al. (2012) analysed raw interface data which partly reflect the systematic changes of modal composition within the rock-fragment assemblage. Our analysis showed these modal trends to be broadly consistent among plutons, which implies that raw interface data would be systematically overprinted. A biplot of the raw interface data which brings out this overprint is shown in Fig. 9. The perceived order of stability extracted from raw interface data may thus be largely explained by the evolution of the modal (mineral) composition from parents to derived sediments (Fig. 7).

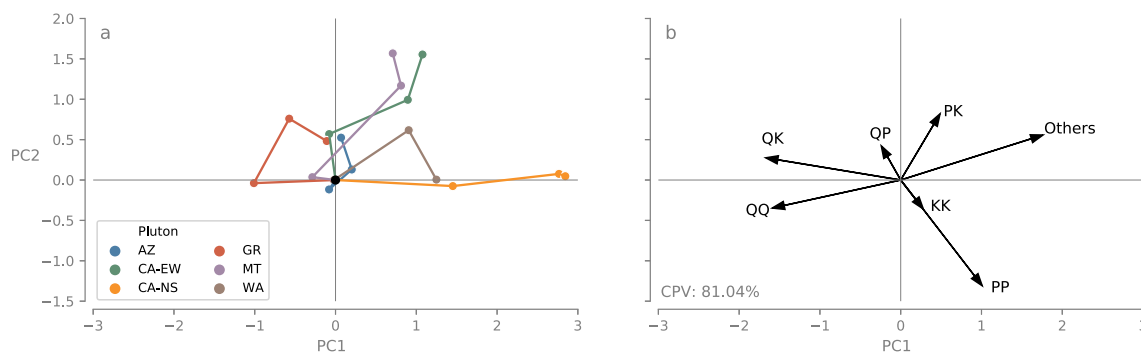


Fig. 9. a) Biplots of weighted “filtered” mean SGE trajectories of raw interface data (without correction for expected interface proportions). The three data points show the composition of coarse-medium-fine sand fractions corrected for the average composition of their parents (black dot). b) PCA loadings of a). Comparison with Fig. 7c and f clearly brings out the overprint of modal composition (property 1) on raw interface data.

6.6. Future research

Geostatistical analysis of property 1 across five plutons (Weltje and Paredis, this issue) indicates that up to several hundreds of specimens must be analysed to obtain accurate estimates of the mean (area-weighted) value of this property, and the same may hold for the other four properties as well. If this is indeed the case, the plutons in the data set presented here have been distinctly undersampled, and thus a high degree of uncertainty must be assigned to the average parent-rock and sediment properties reported above. Given the noise in such small data sets, some form of averaging or smoothing of results is likely to lead to a more robust estimation of SGE trajectories.

To model the trends shown in the biplots of Fig. 7, it should be taken into account that the statistical tests listed in Table 2 indicate that differences between the average compositions of *P* and *C* and those of *M* and *F* are in general not significant. This goes for all properties investigated (1a, 1b, and 2). In other words, the properties of the parent cannot be reliably distinguished from those of the coarse sand fraction, and the properties of the medium and fine sand fractions are equally indistinguishable. This suggests that we may further reduce the data set by averaging the properties of *P* and *C*, as well as those of *M* and *F*. We would then be left with only two data points for each pluton, and its SGE trajectory would reduce to a straight line. This form of reduction, which permits fitting of so-called Linear Compositional Process (LCP) models to the data (von Eynatten et al., 2003) is a logical next step in data analysis. Another logical step would be to try to relate the variability of responses (particularly the evolution of interface compositions) to climate and topography (cf. Heins, 1992, 1993, 1995). We will not pursue this here, as the purpose of our study is to demonstrate the functionality of the GGD through exploratory statistical analysis of fundamental properties.

Modelling of SGE trajectories requires large integrated data sets of parent-rock and sediment properties. An efficient protocol for the acquisition of integrated data sets has been developed by Henares et al. (2019), based on coupling of fast non-destructive spectroscopic measurements obtained with in-situ XRF (X-ray fluorescence) and NIR (near-infra-red reflectance) to sets of calibration samples in which properties of interest have been measured using conventional lab techniques. Partial Least Squares Regression is used to generate a set of calibration equations from which values of the desired properties may be predicted at locations where only spectroscopic data are available. A promising direction of future research is to combine this property-prediction workflow with multivariate geostatistical modelling techniques (Weltje and Paredis, this issue) for the purpose of quantitatively mapping and characterizing entire lithosomes in an efficient way.

Disintegration of rocks along crystal interfaces has not been widely studied from a quantitative point of view. The exploratory analysis of the evolution of interface composition indicates that calibration on a

case-by-case basis is needed for SGE studies in view of the variability of relative interface stabilities among plutons. An additional complication for establishing reliable SGE models that predict the evolution of interface composition is that mechanical and chemical weathering in natural systems go hand in hand, and their interactions are likely to influence overall interface strengths (Pye, 1985, 1986). Therefore, the way forward would be to study sediments with different SGE trajectories generated from a single, preferably homogeneous parent, so as to shed light on relative mineral and interface stabilities under different scenarios of chemical relative to mechanical weathering.

An example of multiple SGE trajectories originating from a single parent was presented by Ibbeken and Schleyer (1991), who investigated the evolution of property 1 by proxy, in the form of bulk chemical composition. They analysed weathering products of the same parent rocks generated under vastly different conditions in the Aspromonte Mountains (South Calabria, Italy). The main conclusion of Ibbeken and Schleyer (1991) is that southern-Calabrian river-mouth sands cannot be regarded as products of chemical weathering *in situ* (soil formation), because their chemical composition does not match that of the soils, and the volumetric contribution of soil material to fluvial sands is negligible. Instead, the bulk composition of sands closely matches that of the parent rocks, which implies that they must have been produced by mechanical grinding in the coarse-grained braided river systems during river floods following major rainstorms. Therefore, the southern-Calabrian rivers have been described as “sediment mills” in which mechanical weathering is the overwhelming control on sediment generation (Ibbeken and Schleyer, 1991). In areas such as these, SGE trajectories of relative interface stabilities under conditions of pure mechanical weathering obtained from the river sands may be compared to those displayed by the sandy soils, which should mainly reflect *in situ* chemical weathering. Studies of this type will be essential for constraining the possible relationship between the evolution of interface composition and environmental factors.

Declaration of Competing Interest

The authors declare that they have no known competing financial interests or personal relationships that could have appeared to influence the work reported in this paper.

Acknowledgements

We wish to acknowledge the achievements of John Cedric Griffiths (1912-1992), Andrei Borisovich Vistelius (1915-1995), and John Aitchison (1926-2016), three titans of mathematical petrology and statistics. Our attempt to quantify sediment properties for the purpose of SGE studies was inspired by their ideas. We thank the editor (Chris Fielding), guest editor (Luca Caracciolo), and two anonymous reviewers

for their valuable suggestions which led to significant improvement of the original manuscript. BP wishes to thank Luca Caracciolo for lending him the thin sections of the parent rocks analysed by WAH. The

research reported here forms part of the PhD thesis of BP, which was funded by KU Leuven.

Appendix A. Stereological inversion

Crystal-size probability distributions (CSPDs) of the parent rocks sampled by Heins (1992) were constructed by combining his 1-D measurements with newly acquired 2-D image analysis data of the same thin sections. In order to reduce the considerable workload of estimating more than 300 crystal-size probability distributions according to the conventional approach (Higgins, 2000, 2006a), we designed an efficient workflow aimed at providing first-order estimates of CSPDs with much less effort. Reduction of the workload was made possible by adopting two assumptions: crystals are approximately spherical and crystal-size frequency follows a lognormal distribution.

A.1. Lognormal distribution

The lognormal distribution may be viewed as the default model for positive quantities which do not possess an upper bound, such as discharge, permeability, or particle size. By definition, crystal size (D) follows a lognormal distribution if $\ln(D)$ follows a normal distribution. Because lognormal distributions are always right-skewed, the arithmetic mean of crystal size \bar{D}_A is always larger than the geometric mean \bar{D}_G . The latter is equal to the arithmetic mean of the logarithms of size after exponentiation:

$$\bar{D}_G = \left(\prod_{i=1}^n D_i \right)^{\frac{1}{n}} = \exp \left\{ \frac{1}{n} \sum_{i=1}^n \ln D_i \right\}$$

$$\bar{D}_A = \frac{1}{n} \sum_{i=1}^n D_i$$

The difference between the two measures of central tendency is a function of the standard deviation of the lognormal distribution. If we define θ as the arithmetic mean and ω as the standard deviation of the normal distribution of $\ln(D)$, and μ as the arithmetic mean of the lognormal distribution of D , ($\mu = \bar{D}_A$) the following fundamental relation applies:

$$\ln \mu = \theta + \frac{\omega^2}{2}$$

$$\text{Where } \theta = \frac{1}{n} \sum_{i=1}^n \ln D_i, \text{ and } \mu = \frac{1}{n} \sum_{i=1}^n D_i.$$

We solve the above equation for θ by estimating μ from the modal and interface data of Heins (1992), and ω from newly acquired digital image-analysis data from the same set of thin sections. This permits the complete crystal-size probability distribution in terms of D to be generated from the normal distribution of $\ln(D)$. A battery of statistical tests (Table 3) was employed to examine if the lognormal distribution provides an adequate explanation of the observations.

A.2. Estimating the arithmetic mean of crystal size

The data set of Heins (1992) comprises interface frequencies, the number of traverses passed when counting the interfaces, and the total traverse length. Hence, the mineral number frequencies n_j may be calculated from the interface frequencies (f) or by summing the entries of the transition matrix row- or column-wise (Weltje et al., 2018). The mean intercept length for each mineral class ($\mu_{1,j}$) is given by:

$$\mu_{1,j} = \frac{\langle x_j \rangle L}{n_j}$$

Where $\langle x_j \rangle$ is the modal proportion of mineral j and L is the total traverse length.

The mean intercept lengths $\mu_{1,j}$ represent a 1-D measure which must be converted to 3-D to give the mean crystal size. Under the assumption that all crystals are spherical, the conversion factor for moving up one dimension is $4/\pi$ (Chayes, 1950; Peterson, 1996) and the mean 3-D diameter may be obtained from:

$$\mu_3 = \frac{4\mu_2}{\pi} = \frac{16\mu_1}{\pi^2}$$

It should be noted that $\mu_{1,j}$, the arithmetic mean intercept length of mineral j obtained from the interface counts of Heins (1992), is based on several thousands of observations in each thin section (see Table 1). The lower limit of resolution of the interface counts of Heins (1992) is 10 µm, which implies that left-hand truncation effects will be small given the large average crystal size of most minerals in granitoids. The predicted 3-D diameter (μ_3) thus serves as a robust measure of central tendency of the crystal-size probability distribution. However, bias may be introduced by the assumption that crystals are well approximated by spheres, which is unlikely to apply to all mineral classes (e.g., micas).

Fitting of a single CSPD by pooling all crystals belonging to the j -th mineral class observed in a set of q thin sections from a given pluton involves the calculation of a weighted arithmetic mean crystal size ($\bar{D}_{p,j}$) from the data:

$$\bar{D}_{p,j} = \frac{\sum_{i=1}^q n_{ij} \mu_{3,ij}}{\sum_{i=1}^q n_{ij}}$$

A.3. Bias correction for thin-section observations

The probability distribution of apparent (2-D) crystal diameters observed in thin or plane section is biased because the probability of selecting a crystal by spatially random sampling depends on its size and on the dimensions of the specimen. The probability of observing a crystal in a finite area (such as a rectangular thin section) can be modelled as the combination of two effects: left-hand and right-hand truncation. Under conditions of spatially uniform random sampling, the left-hand truncation effect is represented by the probability of selecting a crystal with area A in a thin section with length L and width W , where $L \geq W$ by definition:

$$p_{lht} = \frac{A}{LW}$$

This equation depicts the effect of left-hand truncation ($= lht$), i.e., the probability of selecting a crystal vanishes when its area A goes to zero. In practice, p_{lht} equals zero for any crystals smaller than the lower detection limit. For circles, the left-hand truncation effect may be written as:

$$p_{lht} = \frac{\pi D_2^2}{4LW}$$

If we would have carried out an infinite number of random selections which resulted in the identification of a given crystal and recorded the values of all coordinate pairs that fell on it, we would find that the average of the coordinate pairs coincides exactly with the centre of mass of that crystal as observed on the plane. Because we assume that all crystals are spheres, the expected set of coordinates corresponding to each crystal marks the centre of a circle observed on the plane. The right-hand truncation ($= rht$) effect can thus be modelled as the ratio of the area containing feasible locations of circle centres and the total area of the specimen (see Fig. A1):

$$p_{rht} = \frac{(L - D_2)(W - D_2)}{LW}$$

The probability of selecting a crystal goes to zero when its circle diameter approaches the width of the thin section. The relative probability of selecting a circle completely enclosed by the area of the thin section is given by the product of the left- and right-hand truncation probabilities:

$$p_s = p_{lht} p_{rht} = \frac{\pi D_2^2 (L - D_2)(W - D_2)}{4L^2 W^2}$$

This function is equal to zero for crystals at the physical limits of observation (i.e., $D_{\min} = 0$, $D_{\max} = W$), and positive for diameters within this interval. The description is complete if we add the conditions:

$$\begin{aligned} p_s &= 0 && \text{if } D_2 \leq D_{\text{ldl}} \\ p_s &= 0 && \text{if } D_2 \geq W \end{aligned}$$

Where D_{ldl} represents the lower detection limit of the data-acquisition scheme (around 25 µm in our case). The function is symmetrical in the case $L = W$. For a given number of observed crystals (n), the selection probabilities assigned to individual crystals in thin section are:

$$p_{s,i} = \frac{D_{2,i}^2 (L - D_{2,i})(W - D_{2,i})}{\sum_{i=1}^n D_{2,i}^2 (L - D_{2,i})(W - D_{2,i})}$$

The inverse of this distribution is termed the truncation probability:

$$p_{T,i} = \frac{p_{s,i}^{-1}}{\sum_{i=1}^n p_{s,i}^{-1}}$$

The cumulative distribution of p_T gives the corrected probabilities that have to be assigned to observed crystals. It is calculated as:

$$P_{T,h} = \frac{(2n - 1)}{2n} \frac{\sum_{i=1}^h p_{T,i}}{\sum_{i=1}^n p_{T,i}}$$

The term containing n is a continuity correction, which prevents the largest element from being assigned to the highest percentile (i.e., the largest crystal actually observed would have been equated to the maximum crystal size), and is needed to numerically stabilize the estimation procedure (explained in section A5). The distribution of D_2 versus P_T represents the cumulative probability distribution of equivalent circle diameters in the range $D_{\text{ldl}} < D_2 < W$ that would have been observed in a thin section of infinite size ($W \rightarrow \infty$).

A.4. Stochastic simulation of sectioning

Stochastic simulations of the sectioning process were conducted in which sets of lognormally distributed spheres (with diameters D_3) were cut by random planes to form sets of circles (with diameters D_2). This approach is similar to the techniques used for generating 2-D visual comparators to assess the degree of sorting of phi-normal grain-size distributions in thin section (Longiaru, 1987; Jerram, 2001).

The 3-D lognormal probability density function was initialized with a mean of 0 and a variance ranging from 0.1 to 10 with intervals of 0.1. Note that the mean and variance of the lognormal distribution as defined here are those of the normal distribution of $\ln(D)$. For every interval of the variance, ten simulations were run, resulting in 1000 simulations in total. In every simulation, 100,000 spheres were randomly selected from 100 million spheres.

The first step of the simulation consists of selecting the spheres to be cut. If a set of n spheres is assumed to be randomly distributed in space, the

probability of intersecting a sphere by a random plane is proportional to its diameter:

$$p_{C,i} = \frac{D_{3,i}}{\sum_{i=1}^n D_{3,i}}$$

The intersection probabilities are assigned to each set of n simulated spheres to form the cumulative distribution:

$$P_{C,h} = \frac{\sum_{i=1}^h p_{C,i}}{\sum_{i=1}^n p_{C,i}}$$

The apparent size of the circles on the plane of intersection is modelled by assuming that each sphere is cut according to a random uniform distribution on the interval between its centre and its surface. If n goes to infinity, the expected circle diameter of each sphere is equal to:

$$E(D_2) = \frac{\pi D_3}{4}$$

The result of the stochastic simulation is the probability distribution of circle diameters that will be observed on a plane of infinite size if the spheres follow a lognormal distribution and are randomly distributed in space. The stochastic simulation is illustrated in Fig. A2.

A.5. Estimating the standard deviation

After correcting for the effects of truncation, the 2-D data obtained from digital image analysis of the thin sections have been transformed into a cumulative probability distribution of circle diameters observed on an infinite plane. This representation coincides with the format in which the output of the stochastic simulations is given. Hence, data and model may be directly compared and ω (the standard deviation of the best-fit lognormal distribution) may be estimated from the cumulative probability distribution of the corrected data.

The cumulative probability distribution of $\ln(D_2)$ resulting from the simulations is far from linear (Fig. A2). A rough linearization was achieved by transforming the cumulative probability P to an additive log-ratio (also known as logit):

$$P_{0,i} = \ln\left(\frac{P_i}{1 - P_i}\right)$$

Note that the above transformation implies that all values of P must be larger than zero and smaller than unity (hence the continuity correction). The values of $P_{0,i}$ were centred about the origin to form:

$$\tilde{q}_i = P_{0,i} - \frac{1}{n} \sum_{i=1}^n P_{0,i}$$

In the next step, \tilde{q} was further modified to form q :

$$q_i = \text{sign}(\tilde{q}_i) \cdot |\tilde{q}_i|^z$$

The value $z = 0.94$ produced a nearly straight line for the cumulative distribution function of $\ln(D)$ versus q within the probability range of [0.05, 0.95]. These limits were adopted to minimize the effect of noise in the tails of the distribution.

The intercept of the straight line was set to zero by subtracting the mean of $\ln(D_2)$ from the observed diameters:

$$\ln(D_{c,i}) = \ln(D_{2,i}) - \frac{1}{n} \sum_{i=1}^n \ln(D_{2,i})$$

As a result of the above operations, the centred cumulative distribution can be closely approximated by a linear function of the following form:

$$q = v \ln(D_c)$$

The slope of this curve, v , is inversely proportional to the standard deviation of the 2-D data, and a monotonic function of the standard deviation of the 3-D data, ω . Fig. A3 shows an example (3-D distribution with mean = 0.0, standard deviation = 1.0).

The relation between v and ω was obtained from the stochastic simulations. Fig. A4 shows that it is well approximated by a power-law function:

$$\omega = 1.628v^{-1.235}$$

This equation may be used to estimate the standard deviation of the lognormal distribution of 3-D crystal sizes from the set of observed 2-D circle diameters after transformation of P_T to q_T (analogous to the transformation of P to q) by means of linear regression.

Fig. A5 shows the cumulative distributions of apparent crystal size plotted on the $\ln(D)$ versus q scales for the pooled data. Lognormal distributions should plot as approximately straight lines in this space. Figures of the approximately 300 cumulative CSPDs at the level of individual thin sections are included in the online supplementary materials.

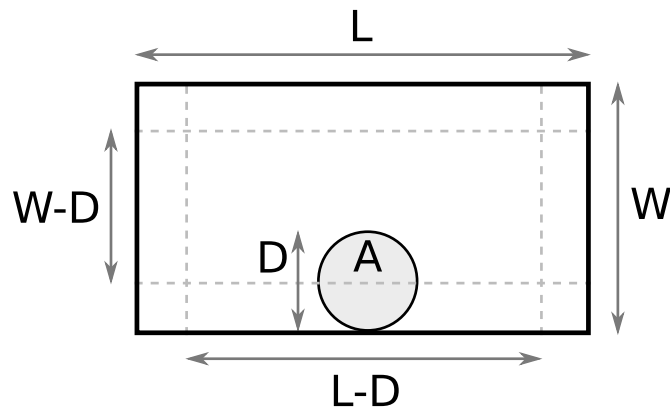


Fig. A1. Schematic overview of data-acquisition parameters used for modelling the left-hand and right-hand truncation effects in thin-section size data.

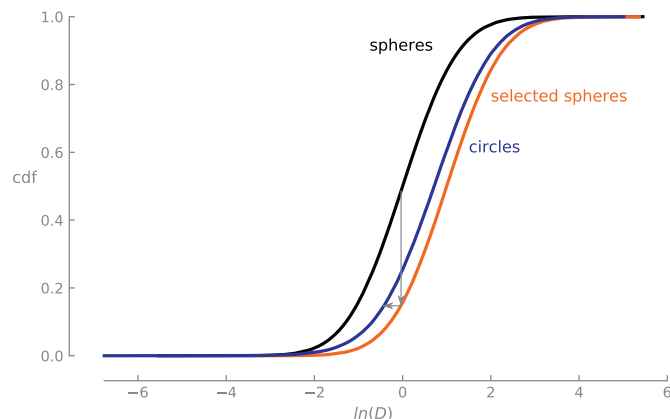


Fig. A2. Simulation of cumulative distribution functions (CDFs) for lognormally distributed spheres (mean = 0.0, standard deviation = 1.0), spheres cut by a random plane, and observed circles on the plane. Arrows mark the transformation from the CDF of spheres to that of selected spheres, and finally to the CDF of circle diameters.

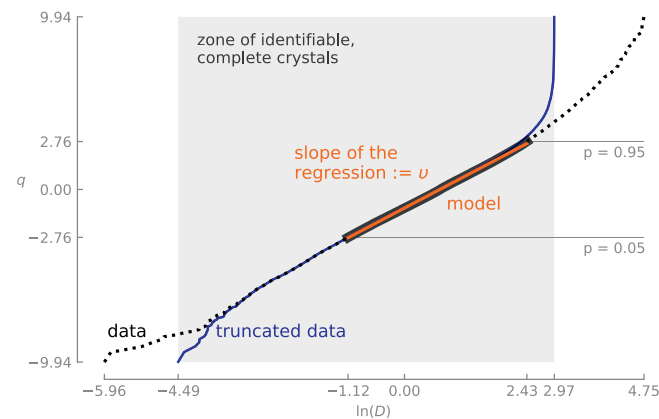


Fig. A3. Between the 0.05 and 0.95 percentiles, a linear relation of $\ln(D)$ with the slope of the cumulative probability distribution (q) supports the assumption of lognormality for a crystal size distribution of circles on an infinite plane. The data were derived from a 3-D distribution with mean = 0.0, standard deviation = 1.0. In this case, left- and right-hand truncation effects owing to resolution limits are very moderate and do not affect the distribution between its 5th and 95th percentile; their importance increases with the standard deviation of the lognormal distribution.

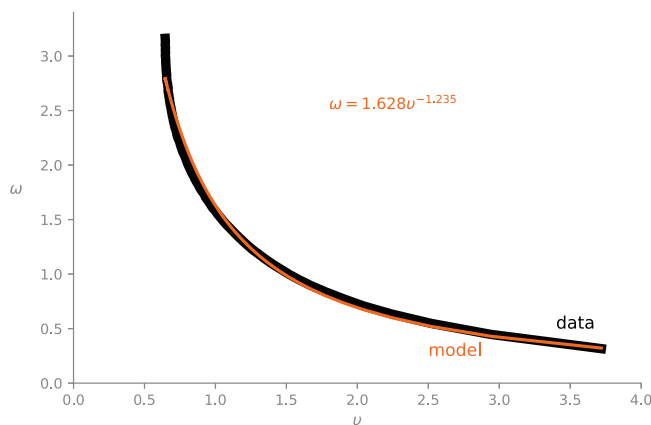


Fig. A4. The power-law relation between v and the 3-D geometric standard deviation (ω) used to convert the 2-D standard deviations to their 3-D equivalents.

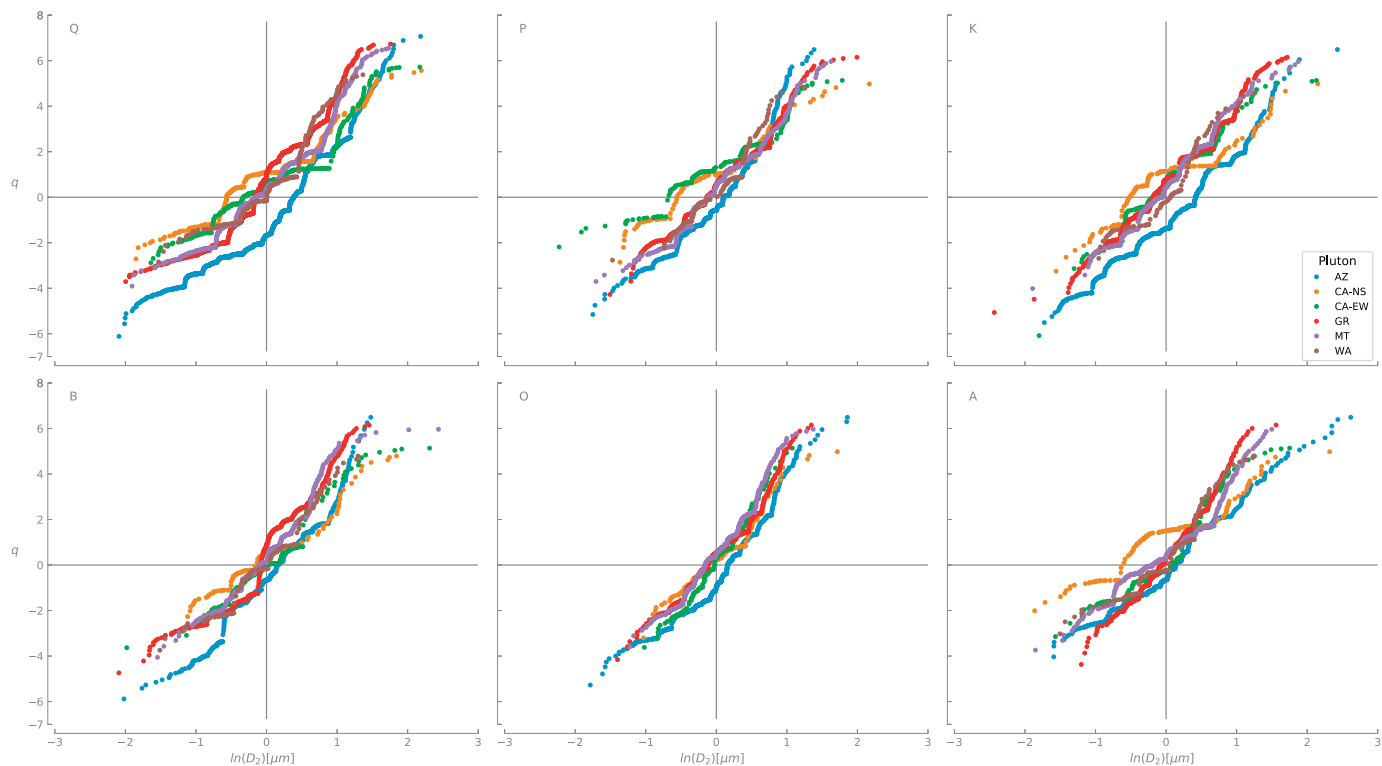


Fig. A5. Cumulative distributions of apparent crystal size plotted on the $\ln(D)$ versus q scales. The relation between $\ln(D)$ and q shows that for most amalgamations of samples per pluton and per mineral class the data follow a straight line indicating lognormality (62% of the distributions is effectively lognormal).

Appendix A. Supplementary data

Supplementary data to this article can be found online at <https://doi.org/10.1016/j.earscirev.2020.103188>.

References

- Aitchison, J., 1982. The statistical analysis of compositional data (with discussion). *Journal of the Royal Statistical Society Series B* 44, 139–177. <https://doi.org/10.1111/j.2517-6161.1982.tb01195.x>.
- Aitchison, J., 1986. *The Statistical Analysis of Compositional Data*. Chapman & Hall, London (416 p.).
- Aitchison, J., Greenacre, M.J., 2002. Biplots of compositional data. *Applied Statistics Series C* 51, 375–392. <https://doi.org/10.1111/1467-9876.00275>.
- Allen, P.A., 2017. Sediment Routing Systems: The Fate of Sediment from Source to Sink. Cambridge University Press <https://doi.org/10.1017/9781316135754>. (422 p.).
- Armenti, P., Tarquini, S., 2002. Power law olivine crystal size distributions in lithospheric mantle xenoliths. *Lithos* 65, 273–285. [https://doi.org/10.1016/S0024-4937\(02\)00195-0](https://doi.org/10.1016/S0024-4937(02)00195-0).
- Barrett, P.J., 1980. The shape of rock particles, a critical review. *Sedimentology* 27, 291–303. <https://doi.org/10.1111/j.1365-3091.1980.tb01179.x>.
- Basu, A., 1985. Influence of climate and relief on compositions of sands released at source areas. In: Zuffa, G.G. (Ed.), *Provenance of Arenites*. NATO-ASI Series D. Reidel, Dordrecht, pp. 1–18. https://doi.org/10.1007/978-94-017-2809-6_1.
- Basu, A., 2003. A perspective on quantitative provenance analysis. In: Valloni, R., Basu, A. (Eds.), *Quantitative Provenance Studies in Italy. Memorie Descrittive della Carta Geologica dell'Italia* 61. pp. 11–22.
- Berger, A., Herwegh, M., Schwarz, J.-O., Putlitz, N., 2011. Quantitative analysis of crystal/grain sizes and their distributions in 2D and 3D. *J. Struct. Geol.* 33, 1751–1763. <https://doi.org/10.1016/j.jsg.2011.07.002>.
- Blott, S.J., Pye, K., 2008. Particle shape: a review and new methods of characterization and classification. *Sedimentology* 55, 31–63. <https://doi.org/10.1111/j.1365-3091.2007.00892.x>.
- Burger, H., Skala, W., 1976. Comparison of sieve and thin-section technique by a Monte-Carlo model. *Comput. Geosci.* 2, 123–139. [https://doi.org/10.1016/0098-3004\(76\)90103-5](https://doi.org/10.1016/0098-3004(76)90103-5).

- Caracciolo, L., Tolosana-Delgado, R., Le Pera, E., von Eynatten, H., Arribas, J., Tarquini, S., 2012. Influence of granitoid textural parameters on sediment composition: Implications for sediment generation. *Sediment. Geol.* 280, 93–107. <https://doi.org/10.1016/j.sedgeo.2012.07.005>.
- Chayes, F., 1950. On the bias of grain-size measurements made in thin section. *J. Geol.* 58, 156–160. <https://doi.org/10.1086/625160>.
- Chayes, F., 1956. *Petrographic Modal Analysis: an Elementary Statistical Appraisal*. Wiley, New York (113 p.).
- Cruz Orive, L.-M., 1976. Particle size-shape distributions: the general spheroid problem, I. Mathematical model. *Journal of Microscopy* 107, 235–253. <https://doi.org/10.1111/j.1365-2818.1976.tb02446.x>.
- Cruz Orive, L.-M., 1978. Particle size-shape distributions: the general spheroid problem, II. Stochastic model and practical guide. *Journal of Microscopy* 112, 153–167. <https://doi.org/10.1111/j.1365-2818.1978.tb01162.x>.
- Curry, J.R., Griffiths, J.C., 1955. Sphericity and roundness of quartz grains in sediments. *Bull. Geol. Soc. Am.* 66, 1075–1096. [https://doi.org/10.1130/0016-7606\(1955\)66\[1075:SAROQG\]2.0.CO;2](https://doi.org/10.1130/0016-7606(1955)66[1075:SAROQG]2.0.CO;2).
- Davis, J.C., 2002. *Statistics and Data Analysis in Geology*, Third edition. Wiley, New York (656 p.).
- Dickinson, W.R., 1985. Interpreting provenance relations from detrital modes of sandstones. In: Zuffa, G.C. (Ed.), *Provenance of Arenites*. D. Reidel Publishing Company Dordrecht, The Netherlands, pp. 333–362. https://doi.org/10.1007/978-94-017-2809-6_15.
- Diepenbroek, M., Bartholomae, A., Ibbeken, H., 1992. How round is round? A new approach to the topic ‘roundness’ by Fourier grain shape analysis. *Sedimentology* 39, 411–422. <https://doi.org/10.1111/j.1365-3091.1992.tb02125.x>.
- Elsey, M., Esedoglu, S., Smreka, P., 2011. Large-scale simulation of normal grain growth via diffusion-generated motion. *Proceedings of the Royal Society Series A* 467, 381–401. <https://doi.org/10.1098/rspa.2010.0194>.
- Erkan, Y., 1970. Ein Versuch zur quantitative Erfassung der Festigkeits-eigenschaften und zur quantitative Charakterisierung der Granite. *Neues Jahrbuch für Mineralogie, Abhandlungen* 113, 91–109.
- Fisher, N.I., Lewis, T., Embleton, B.J.J., 1987. *Statistical Analysis of Spherical Data*. Cambridge University Press, Cambridge (329 p.).
- Graham, D.J., Gadsden, R.J., 2019. New statistical methods for the comparison and characterisation of particle shape. *Earth Surf. Process. Landf.* <https://doi.org/10.1002/esp.4669>.
- Griffiths, J.C., 1952. Grain-size distribution and reservoir-rock characteristics. *Bull. Am. Assoc. Pet. Geol.* 36, 205–229. <https://doi.org/10.1306/3d9343ee-16b1-11d7-8645000102c1865d>.
- Griffiths, J.C., 1961. Measurement of the properties of sediments. *J. Geol.* 69, 487–498. <https://doi.org/10.1086/626767>.
- Griffiths, J.C., 1967. *Scientific Method in Analysis of Sediments*. McGraw-Hill, New York (508 p.).
- Harvey, P.K., Ferguson, C.C., 1978. A computer simulation approach to textural interpretation in crystalline rocks. In: Merriam, D.F. (Ed.), *Recent Advances in Geomathematics: An International Symposium*. Pergamon, Oxford, pp. 201–232. <https://doi.org/10.1016/B978-0-08-022095-6.50019-8>.
- Harvey, P.K., Lovell, M.A., 1992. Downhole mineralogy logs: Mineral inversion methods and the problem of compositional collinearity. In: Hurst, A., Griffiths, C.M., Worthington, P.F. (Eds.), *Geological Applications of Wireline Logs*. Geological Society Special Publication 65. pp. 361–368.
- Heins, W.A., 1992. *The Effect of Climate and Topography on the Composition of Modern Plutoniclastic Sand*. University of California, Los Angeles (PhD thesis, 465 p.).
- Heins, W.A., 1993. Source rock texture versus climate and topography as controls on the composition of modern plutoniclastic sand. In: Geological Society of America Special Paper 284, pp. 135–146. <https://doi.org/10.1130/SPE284-p135>.
- Heins, W.A., 1995. The use of mineral interfaces in sand-sized rock fragments to infer ancient climate. *Geol. Soc. Am. Bull.* 107, 113–125. [https://doi.org/10.1130/0016-7606\(1995\)107%3C0113:TUOMII%3E2.3.CO;2](https://doi.org/10.1130/0016-7606(1995)107%3C0113:TUOMII%3E2.3.CO;2).
- Heins, W.A., Kairo, S., 2007. Predicting sand character with integrated genetic analysis. In: Geological Society of America Special Paper 420, pp. 345–380. [https://doi.org/10.1130/2006.2420\(20\)](https://doi.org/10.1130/2006.2420(20)).
- Henaress, S., Donselaar, M.E., Bloemsma, M.R., Tjallingii, R., De Wijn, B., Weltje, G.J., 2019. Quantitative integration of sedimentological core descriptions and petrophysical data using high-resolution XRF core scans. *Mar. Pet. Geol.* 110, 450–462. <https://doi.org/10.1016/j.marpetgeo.2019.07.034>.
- Higgins, M.D., 2000. Measurement of crystal size distributions. *Am. Mineral.* 85, 1105–1116. <https://doi.org/10.2138/am-2000-8-901>.
- Higgins, M.D., 2002. Closure in crystal size distributions (CSD), verification of CSD calculations, and the significance of CSD fans. *Am. Mineral.* 87, 171–175. <https://doi.org/10.2138/am-2002-0118>.
- Higgins, M.D., 2006a. *Quantitative Textural Measurements in Igneous and Metamorphic Petrology*. Cambridge University Press, Cambridge (270 p.).
- Higgins, M.D., 2006b. Verification of ideal semi-logarithmic, lognormal or fractal crystal size distributions from 2D datasets. *J. Volcanol. Geotherm. Res.* 154, 8–16. <https://doi.org/10.1016/j.jvolgeores.2005.09.015>.
- Higgins, M.D., 2010. Imaging birefringent minerals without extinction using circularly polarized light. *Can. Mineral.* 48, 231–235. <https://doi.org/10.3749/canmin.48.1.231>.
- Hilden, M.M., Powell, M.S., 2017. A geometrical texture model for multi-mineral liberation prediction. *Miner. Eng.* 111, 25–35. <https://doi.org/10.1016/j.mineng.2017.04.020>.
- Ibbeken, H., Schleyer, R., 1991. *Source and Sediment: a Case Study of Provenance and Mass Balance at an Active Plate Margin (Calabria, Southern Italy)*. Springer-Verlag, Berlin (286 p.).
- Jerram, D.A., 2001. Visual comparators for degree of sorting in 2-D and 3-D. *Comput. Geosci.* 27, 485–492. [https://doi.org/10.1016/S0098-3004\(00\)00077-7](https://doi.org/10.1016/S0098-3004(00)00077-7).
- Jerram, D.A., Cheadle, M.J., Hunter, R.H., Elliott, M.T., 1996. The spatial distribution of grains and crystals in rocks. *Contrib. Mineral. Petrol.* 125, 60–74. <https://doi.org/10.1007/s004100050206>.
- Johnsson, M.J., 1993. The system controlling the composition of clastic sediments. In: Johnsson, M.J., Basu, A. (Eds.), *Processes Controlling the Composition of Clastic Sediments*. Geological Society of America Special Paper 284pp. 1–19. <https://doi.org/10.1130/SPE284-p1>.
- Johnsson, M.J., Stallard, R.F., Meade, R.H., 1988. First-cycle quartz arenites in the Orinoco River basin, Venezuela and Colombia. *J. Geol.* 96, 263–277. <http://www.jstor.org/stable/30068727>.
- Johnsson, M.J., Stallard, R.F., Lundberg, N., 1991. Controls on the composition of fluvial sands from a tropical weathering environment: Sands of the Orinoco River drainage basin, Venezuela and Colombia. *Geological Society of America Bulletin* 103, 1622–1647. [https://doi.org/10.1130/0016-7606\(1991\)103%3C1622:COTCOF%3E2.3.CO;2](https://doi.org/10.1130/0016-7606(1991)103%3C1622:COTCOF%3E2.3.CO;2).
- Jutzeler, M., Proussevitch, A.A., Allen, S.R., 2012. Grain-size distribution of volcaniclastic rocks 1: a new technique based on functional stereology. *J. Volcanol. Geotherm. Res.* 239–240, 1–11. <https://doi.org/10.1016/j.jvolgeores.2012.05.013>.
- Kahl, W.A., Dilissen, N., Hidas, K., Garrido, C.J., López Sánchez-Vizcaíno, V., Román Alpiste, M.J., 2017. 3-D microstructure of olivine in complex geological materials reconstructed by correlative X-ray μ -CT and EBSD analyses. *J. Microsc.* 268, 193–207. <https://doi.org/10.1111/jmi.12598>.
- Kahn, J.S., 1956. The analysis and distribution of the properties of packing in sand size sediments: I, On the measurement of packing in sandstones. *Journal of Geology* 64, 385–395. <https://doi.org/10.1086/626372>.
- Kilian, K., Heilbronner, R., Stünitz, H., 2011. Quartz grain size reduction in a granitoid rock and the transition from dislocation to diffusion creep. *J. Struct. Geol.* 33, 1265–1284. <https://doi.org/10.1016/j.jsg.2011.05.004>.
- Long, H., Swennen, R., Fouquet, A., Dierick, M., Jacobs, P., 2009. 3D quantification of mineral components and porosity distribution in Westphalian C sandstone by microfocus X-ray computed tomography. *Sediment. Geol.* 220, 116–125. <https://doi.org/10.1016/j.sedgeo.2009.07.003>.
- Longiaru, S., 1987. Visual comparators for estimating the degree of sorting from plane and thin section. *J. Sediment. Res.* 57, 791–794. <https://doi.org/10.1306/212F8C60-2B24-11D7-8648000102C1865D>.
- Marschallinger, R., 2001. Three-dimensional reconstruction and visualization of geological materials with IDL – examples and source code. *Comput. Geosci.* 27, 419–426. [https://doi.org/10.1016/S0098-3004\(00\)00126-6](https://doi.org/10.1016/S0098-3004(00)00126-6).
- Marsh, B.D., 1988. Crystal size distribution (CSD) in rocks and the kinetics and dynamics of crystallization. *Contrib. Mineral. Petrol.* 99, 277–291. <https://doi.org/10.1007/BF00375362>.
- McCanta, M.C., Dyr, M.D., Dobosh, P.A., 2017. Extracting bulk rock properties from microscale measurements: subsampling and analytical guidelines. *GSA Today* 27, 4–9. <https://doi.org/10.1130/GSATG290A.1>.
- McEwen, M.C., Fessenden, F.W., Rogers, J.J.W., 1959. Texture and composition of some weathered granites and slightly transported arkosic sands. *J. Sediment. Petrol.* 29, 477–492. <https://doi.org/10.1306/74D7097A-2B21-11D7-8648000102C1865D>.
- Miyoshi, E., Takaki, T., Ohno, M., Shibuta, Y., Sakane, S., Shimokawabe, T., Aoki, T., 2017. Ultra-large-scale phase-field simulation study of ideal grain growth. *NPJ Computational Materials* 3, 25. <https://doi.org/10.1038/s41524-017-0028-8>.
- Morishita, R., 1998. Statistical properties of ideal rock textures: relationship between crystal size distribution and spatial correlation of minerals. *Math. Geol.* 30, 409–434. <https://doi.org/10.1023/A:1021796208079>.
- Morishita, R., Obata, M., 1995. A new statistical description of the spatial distribution of minerals in rocks. *J. Geol.* 103, 232–240. <https://doi.org/10.1086/629739>.
- Moss, A.J., 1966. Origin, shaping and significance of quartz sand grains. *J. Geol. Soc. Aust.* 13, 97–136. <https://doi.org/10.1080/0016716608728607>.
- Nesbitt, H.W., 2003. Petrogenesis of siliciclastic sediments and sedimentary rocks. In: Lenz, D.R. (Ed.), *Geochemistry of Sediments and Sedimentary Rocks*, Geotext 4. Geological Association of Canada, Newfoundland, pp. 39–51.
- Nesbitt, H.W., Young, G.M., 1996. Petrogenesis of sediments in the absence of chemical weathering: effects of abrasion and sorting on bulk composition and mineralogy. *Sedimentology* 43, 341–358. <https://doi.org/10.1046/j.1365-3091.1996.d01-12.x>.
- Pawlowsky-Glahn, V., Egozcue, J.J., Tolosana-Delgado, R., 2015. *Modeling and Analysis of Compositional Data*. Wiley, Chichester. <https://doi.org/10.1002/9781119003144>. (272 p.).
- Paxton, S.T., Szabo, J.O., Ajdukiewicz, J.M., Klimentidis, R.E., 2002. Construction of an intergranular volume compaction curve for evaluating and predicting compaction and porosity loss in rigid-grain sandstone reservoirs. *Bull. Am. Assoc. Pet. Geol.* 86, 2047–2067. <https://doi.org/10.1306/61eeddfa-173e-11d7-8645000102c1865d>.
- Peterson, T.D., 1996. A refined technique for measuring crystal size distributions in thin section. *Contrib. Mineral. Petrol.* 124, 395–405. <https://doi.org/10.1007/s004100050199>.
- Potter, P.E., 1986. South America and a few grains of sand: part 1 - beach sands. *J. Geol.* 94, 301–319. <https://www.jstor.org/stable/30068707>.
- Proussevitch, A.A., Sahagian, D.L., Carlson, W.D., 2007a. Statistical analysis of bubble and crystal size distributions: application to Colorado Plateau basalts. *J. Volcanol. Geotherm. Res.* 164, 112–126. <https://doi.org/10.1016/j.jvolgeores.2007.04.006>.
- Proussevitch, A.A., Sahagian, D.L., Tsentalovich, E.P., 2007b. Statistical analysis of bubble and crystal size distributions: formulations and procedures. *J. Volcanol. Geotherm. Res.* 164, 95–111. <https://doi.org/10.1016/j.jvolgeores.2007.04.007>.
- Pye, K., 1985. Granular disintegration of gneiss and migmatites. *Catena* 12, 191–199. [https://doi.org/10.1016/S0341-8162\(85\)80017-5](https://doi.org/10.1016/S0341-8162(85)80017-5).
- Pye, K., 1986. Mineralogical and textural controls on the weathering of granitoid rocks.

- Catena 13, 47–57. [https://doi.org/10.1016/S0341-8162\(86\)80004-2](https://doi.org/10.1016/S0341-8162(86)80004-2).
- Robin, P.-Y.F., Charles, C.R.J., 2015. Quantifying the three-dimensional shapes of spheroidal objects in rocks imaged by tomography. *J. Struct. Geol.* 77, 1–10. <https://doi.org/10.1016/j.jsg.2015.05.002>.
- Rubey, W.W., 1933. The size distribution of heavy minerals within a water-laid sandstone. *J. Sediment. Petrol.* 3, 3–29. <https://doi.org/10.1306/D4268E37-2B26-11D7-8648000102C1865D>.
- Sahagian, D.L., Proussevitch, A.A., 1998. 3D particle size distributions from 2D observations: stereology for natural applications. *J. Volcanol. Geotherm. Res.* 84, 173–196. [https://doi.org/10.1016/S0377-0273\(98\)00043-2](https://doi.org/10.1016/S0377-0273(98)00043-2).
- Savanick, G.A., Johnson, D.I., 1974. Measurements of the strength of grain boundaries in rock. *Int. J. Rock Mech. Min. Sci. Geomech. Abstr.* 11, 173–180. [https://doi.org/10.1016/0148-9062\(74\)90884-5](https://doi.org/10.1016/0148-9062(74)90884-5).
- Schöpa, A., Floess, D., de Saint Blanquat, M., Annen, C., Launeau, P., 2015. The relation between magnetite and silicate fabric in granitoids of the Adamello Batholith. *Tectonophysics* 642, 1–15. <https://doi.org/10.1016/j.tecto.2014.11.022>.
- Schroeder van der Kolk, J.L.C., 1898. *Bijdrage tot de karteering onzer zandgronden (III)*. Koninklijke Akademie van Wetenschappen Amsterdam, Verhandelingen, tweede sectie 6 (4) 23 p.
- Schultz, E.H., 1982. The chromosome and supersome: terms proposed for low-rank chronostratigraphic units. *Bull. Can. Petrol. Geol.* 30, 29–33.
- Sharp, W.E., Severance, K., 1991. Reversible Markov grain sequences in granite. *Math. Geol.* 23, 305–324. <https://doi.org/10.1007/BF02065785>.
- Simmons, G., Richter, D., 1976. Microcracks in Rocks. In: Strens, R.G.J. (Ed.), *The Physics and Chemistry of Minerals and Rocks*. Wiley, London, pp. 105–137.
- Stephens, M.A., 1974. EDF statistics for goodness of fit and some comparisons. *J. Am. Stat. Assoc.* 69, 730–737. <https://doi.org/10.1080/01621459.1974.10480196>.
- Suttner, L.J., Dutta, P.K., 1986. Alluvial sandstone composition and palaeoclimate: framework mineralogy. *J. Sediment. Petrol.* 56, 329–345. <https://doi.org/10.1306/212F8909-2B24-11D7-8648000102C1865D>.
- Tarquini, S., Favalli, M., 2010. A microscopic information system (MIS) for petrographic analysis. *Comput. Geosci.* 36, 665–674. <https://doi.org/10.1016/j.cageo.2009.09.017>.
- van den Boogaart, K.G., Tolosana-Delgado, R., 2013. Analysing compositional data with R. Springer, Heidelberg. <https://doi.org/10.1007/978-3-642-36809-7>. (258 p.).
- Van der Wielen, K.P., Rollinson, G., 2016. Texture-based analysis of liberation behavior using Voronoi tessellations. *Miner. Eng.* 89, 93–107. <https://doi.org/10.1016/j.mineng.2015.09.008>.
- Vistelius, A.B., 1972. Ideal granite and its properties. I: the stochastic model. *Math. Geol.* 4, 89–102. <https://doi.org/10.1007/BF02080295>.
- von Eynatten, H., Barcelo-Vidal, C., Pawlowsky-Glahn, V., 2003. Modeling compositional change: the example of chemical weathering of granitoid rocks. *Math. Geol.* 35, 231–251. <https://doi.org/10.1023/A:1023835513705>.
- von Eynatten, H., Tolosana-Delgado, R., Karius, V., 2012. Sediment generation in modern glacial settings: Grain-size and source-rock control on sediment composition. *Sediment. Geol.* 280, 80–92. <https://doi.org/10.1016/j.sedgeo.2012.03.008>.
- von Eynatten, H., Tolosana-Delgado, R., Karius, V., Bachmann, K., Caracciolo, L., 2016. Sediment generation in humid Mediterranean setting: Grain-size and source-rock control on sediment geochemistry and mineralogy (Sila Massif, Calabria). *Sediment. Geol.* 336, 68–80. <https://doi.org/10.1016/j.sedgeo.2015.10.008>.
- Wang, Y., 2015. Numerical modelling of heterogeneous rock breakage behaviour based on texture images. *Miner. Eng.* 74, 130–141. <https://doi.org/10.1016/j.mineng.2014.12.030>.
- Weltje, G.J., 2012. Quantitative models of sediment generation and provenance: state of the art and future developments. *Sediment. Geol.* 280, 4–20. <https://doi.org/10.1016/j.sedgeo.2012.03.010>.
- Weltje, G.J., Brommer, M.B., 2011. Sediment-budget modelling of multi-sourced basin fills: application to recent deposits of the western Adriatic mud wedge (Italy). *Basin Res.* 23, 291–308. <https://doi.org/10.1111/j.1365-2117.2010.00484.x>.
- Weltje, G.J., von Eynatten, H., 2004. Quantitative provenance analysis of sediments: review and outlook. *Sediment. Geol.* 171, 1–11. <https://doi.org/10.1016/j.sedgeo.2004.05.007>.
- Weltje, G.J., Paredis, B., Caracciolo, L., Heins, W.A., 2018. Quantitative analysis of crystal-interface frequencies in granitoids: implications for modelling of parent-rock texture and its influence on the properties of plutoniclastic sands. *Sediment. Geol.* 375, 72–85. <https://doi.org/10.1016/j.sedgeo.2018.01.004>.
- Whitten, E.H.T., Dacey, M.F., 1975. On the significance of certain Markovian features of granite textures. *J. Petrol.* 16, 429–453. <https://doi.org/10.1093/petrology/16.1.429>.
- Wu, W., Wang, S.S.Y., 2006. Formulas for sediment porosity and settling velocity. *J. Hydraul. Eng.* 132, 858–862. [https://doi.org/10.1061/\(ASCE\)0733-9429\(2006\)132:8\(858\)](https://doi.org/10.1061/(ASCE)0733-9429(2006)132:8(858)).
- Youd, T.L., 1985. Factors controlling maximum and minimum densities of sands. In: Selig, E.T., Ladd, R.S. (Eds.), *Evaluation of relative density and its role in geotechnical projects involving cohesionless soils*. Symposium at the 75th annual meeting, Los Angeles, June 1972 253. ASTM Special Technical Publication, pp. 98–112. <https://doi.org/10.1520/STP37866S>.